Next-to-leading-order electroweak corrections to pp → W⁺W⁻ → 4 leptons at the LHC

B. Biedermann,[a] **M. Billoni,**[b] **A. Denner,**[a] **S. Dittmaier,**[c] **L. Hofer,**[d] **B. Jäger**[b] **and L. Salfelder**[b]

[a]*Institut für Theoretische Physik und Astrophysik, Julius-Maximilians-Universität Würzburg,*
97074 Würzburg, Germany

[b]*Institut für Theoretische Physik, Eberhard Karls Universität Tübingen,*
72076 Tübingen, Germany

[c]*Physikalisches Institut, Albert-Ludwigs-Universität Freiburg,*
79104 Freiburg, Germany

[d]*Department de Física Quàntica i Astrofísica (FQA), Institut de Ciències del Cosmos (ICCUB),*
Universitat de Barcelona (UB),
08028 Barcelona, Spain

E-mail: benedikt.biedermann@physik.uni-wuerzburg.de,
marina.billoni@gmail.com, ansgar.denner@physik.uni-wuerzburg.de,
stefan.dittmaier@physik.uni-freiburg.de, hofer@ecm.ub.edu,
barbara.jaeger@itp.uni-tuebingen.de,
lukas.salfelder@uni-tuebingen.de

ABSTRACT: We present results of the first calculation of next-to-leading-order electroweak corrections to W-boson pair production at the LHC that fully takes into account leptonic W-boson decays and off-shell effects. Employing realistic event selections, we discuss the corrections in situations that are typical for the study of W-boson pairs as a signal process or of Higgs-boson decays H → WW*, to which W-boson pair production represents an irreducible background. In particular, we compare the full off-shell results, obtained treating the W-boson resonances in the complex-mass scheme, to previous results in the so-called double-pole approximation, which is based on an expansion of the loop amplitudes about the W resonance poles. At small and intermediate scales, i.e. in particular in angular and rapidity distributions, the two approaches show the expected agreement at the level of fractions of a percent, but larger differences appear in the TeV range. For transverse-momentum distributions, the differences can even exceed the 10% level in the TeV range where "background diagrams" with one instead of two resonant W bosons gain in importance because of recoil effects.

Contents

1 Introduction

In the second phase of data taking at the LHC, which has started in 2015 with a centre-of-mass (CM) energy of $13\,\text{TeV}$ (almost twice the energy available before) and a target luminosity of several $100\,\text{fb}^{-1}$, the experimental analyses of many electroweak (EW) processes are continued both with a deeper energy reach into the TeV range and with higher statistics at intermediate energies. This, in particular, applies to W-boson pair production, which is not only interesting as signal process but also as background to many searches for new physics and to precision studies of the recently discovered Higgs boson in its WW* decay channel.

As signal process, W-pair production is an optimal test-ground for the triple-gauge-boson interaction of two W bosons with a photon or a Z boson, which is sensitive to physics beyond the Standard Model (SM) especially at high energies. Already the experimental analyses of ATLAS [1, 2] and CMS [3, 4] at Run 1 of the LHC provided constraints on non-standard γWW and ZWW couplings that are competitive with the results of their predecessor experiments at the p$\bar{\text{p}}$ collider Tevatron and the e$^+$e$^-$ collider LEP, but Run 2 of the LHC will further tighten the existing limits. As background, W-pair production is most prominent in the Higgs production channel $\text{pp} \rightarrow \text{H} \rightarrow \text{WW}^*$, which did not only play an essential role in the Higgs-boson discovery, but will provide important information in precision studies of the coupling of the Higgs boson to the W boson. To this end, both Higgs signal and irreducible WW* background have to be precisely known, in particular

for invariant masses below the W-pair production threshold, where at least one of the W bosons is off its mass shell.

The above-mentioned phenomenological issues call for theoretical predictions for W-pair production at the LHC at the highest possible precision, which carefully take into account decay and off-shell effects of the W bosons including fully differential kinematics and phase-space regions below the W-pair threshold. In order to reach an accuracy at the few-percent level, radiative corrections of both the strong and EW interactions have to be calculated and properly combined.

At leading order (LO), W-pair production at hadron colliders is dominated by quark-antiquark annihilation, $q\bar{q} \to WW \to 4\,\text{fermions}$. The largest corrections at next-to-leading order (NLO) result from QCD. They were first calculated for on-shell W bosons in ref. [5, 6], later refined by including leptonic W decays [7, 8], and implemented in the Monte Carlo program MCFM [9]. As a first step beyond NLO QCD, the NLO predictions were matched to parton-shower programs without [10] and including [11–15] leptonic W decays. Recently, complete next-to-next-to-leading order (NNLO) QCD predictions were presented [16, 17] after a continuous effort over several years [18, 19]. Pushing up the inclusive WW cross section at the LHC by about 9% (12%) at a CM energy of 7(14) TeV with respect to NLO QCD, the NNLO QCD prediction, which has a residual perturbative uncertainty of $\sim 3\%$ in the $q\bar{q}$ channel, widely relaxed a tension between theory predictions for inclusive cross sections and LHC data. In order to sustain an accuracy of a few percent also for fiducial cross sections based on hard selection cuts, QCD resummations should be taken into account, which were carried out in ref. [20–22].

Starting at NNLO, W-boson pairs can also be produced in gluon-gluon scattering via quark loops, $gg \to WW$, a channel that is enhanced by the large gluon flux at the LHC and is particularly important in predicting the direct WW background to Higgs production. At the one-loop level, this channel was considered for on-shell W bosons in ref. [23, 24] and later refined by including leptonic W decays [25, 26], additional jet production [27], $gg \to WWg \to 4\ell g$, and non-standard couplings [28]. A comprehensive QCD-based prediction for (off-shell) WW production at the LHC, including the gg channel for both WW and WW+jet production, was presented in ref. [29] in a study of these reactions as background to Higgs-boson production. Very recently, the full NLO prediction for $gg \to WW$ with leptonic W-boson decays was presented in the literature [30].

At the accuracy level of a few percent, EW corrections play an important role as well, in particular due to their known enhancement by soft/collinear EW gauge-boson exchange at high energies and by photon emission off final-state leptons. Aiming at energies in the TeV range at the LHC, where EW corrections generically grow to some 10%, in refs. [31–33] EW corrections to W-pair production were first considered in logarithmic approximations at NLO and NNLO. Those predictions, however, are valid only in the Sudakov regime where the absolute values of the Mandelstam variables $\hat{s}, \hat{t}, \hat{u}$ of the W bosons have to be much larger than the square of the W-boson mass M_W. Therefore, the approximations neither apply to low and intermediate energies, nor to the dominant kinematical domain of forward-produced W bosons at high energies. This shortcoming was overcome by complete NLO EW calculations for the production of on-shell W pairs [34–36], which already revealed

large and non-uniform corrections to kinematical distributions. A subsequent evaluation of EW corrections that includes leptonic W decays and off-shell effects in double-pole approximation (DPA) [37] confirmed these large EW corrections and proved their existence in more realistic kinematical distributions of the W decay products. Recently, EW corrections to leptonically decaying W pairs were included in HERWIG [38], however, in an approach that approximately integrates out photons emitted in the WW production process, i.e. their kinematics is not transferred to the events.

The discussion of EW corrections in the literature also includes effects of channels with photons in the initial state (so-called photon-induced channels), both for inelastic [34–37, 39] and elastic [40] WW production. Owing to the huge $\gamma\gamma \to$ WW cross section at large partonic CM energies, the impact of this channel is quite large, in particular in the forward and backward regions in the TeV range. On the other hand, quark-photon channels do not seem to cause significant effects because their impact is swamped by jet radiation from QCD corrections. Generally, it should be noticed that a precise prediction of the photon-induced channels is limited by large uncertainties in the photon distribution function, especially at large momentum fractions $x > 0.1$ of the photon, where uncertainties can be as large as 100% [41]. Future fits of parton densities will certainly improve this situation.

In this paper we further refine the calculations of NLO EW corrections to W-pair production in $q\bar{q}$ annihilation by including leptonic W-boson decays and all off-shell effects of intermediate W bosons, comprising, in particular, diagrammatic topologies without intermediate W pairs ("background diagrams"). The presented calculation is thus the first that accounts for EW corrections to the cross section at partonic CM energies $\sqrt{\hat{s}}$ below the WW threshold at $2M_\mathrm{W}$, an issue that, since $M_\mathrm{H} < 2M_\mathrm{W}$, is particularly interesting in predicting the WW background to Higgs-boson production in the H $\to$ WW* channel. Note, however, that the inclusion of corrections to the background diagrams without intermediate WW states is expected to be very interesting at high scattering energies as well. This can be deduced from the comparison of the full off-shell NLO prediction for $\mathrm{e^+e^-} \to 4\,$fermions [42, 43] with results in double-pole approximation as delivered by the Monte Carlo program RACOONWW [44–46]. While the double-pole approximation is accurate within $\sim 0.5\%$ for scattering energies $\lesssim 500\,\mathrm{GeV}$, the differences to the full calculation increase for higher energies. It will be interesting to perform this comparison for LHC observables which reach deeply into the TeV range.

In practice, the calculation of NLO EW corrections to pp $\to 4\,$fermions is complex for various reasons. We have performed two completely independent evaluations of all ingredients in order to guarantee reliable and accurate results, similar to our NLO calculation for the process pp $\to \mu^+\mu^-\mathrm{e^+e^-} + X$ [47]. Algebraically, the $2 \to 4$ one-loop matrix elements are involved, and an efficient and fast Monte Carlo integration over the four- and five-particle phase spaces is a non-trivial task. One of our matrix-element calculations follows exactly the strategy of refs. [42, 43], the other one is based on RECOLA [48, 49]. To obtain numerically stable results for the loop integrals everywhere in phase space, we use the library COLLIER [50, 51]. Conceptually, NLO calculations to processes involving resonances are difficult because of issues with gauge invariance, since resonance poles are cured

by a partial Dyson summation of self-energy corrections which jeopardizes the validity of gauge-invariance relations. We solve this problem by using the so-called complex-mass scheme [43, 52, 53], which consistently employs complex gauge-boson masses and delivers gauge-invariant results at NLO accuracy everywhere in phase phase.

The paper is organized as follows: in section 2 we briefly review some details of our calculation of EW corrections. In particular, we describe the conceptual difference of the new full off-shell calculation to the previously applied double-pole approximation. Our phenomenological results are given in section 3, comprising results based on event-selection procedures specifically designed for the investigation of WW final states and Higgs-boson decays $H \to WW^*$, respectively. Section 4, finally, contains our conclusions.

2 Details of the calculation

2.1 Full off-shell calculation

We consider the proton-proton collision process

$$pp \to \nu_\mu \mu^+ e^- \bar{\nu}_e + X, \qquad (2.1)$$

which is dominated by the intermediate state of a pair of potentially resonant W bosons decaying leptonically via $W^+ \to \nu_\mu \mu^+$ and $W^- \to e^- \bar{\nu}_e$. In lowest perturbative order, the process proceeds via the partonic channels

$$\bar{q}q/q\bar{q}/\gamma\gamma \to \nu_\mu \mu^+ e^- \bar{\nu}_e, \qquad (2.2)$$

where the contribution of the $\gamma\gamma$ initial state is typically strongly suppressed with respect to the dominant antiquark-quark ($\bar{q}q/q\bar{q}$) annihilation channels. Figure 1 shows the complete set of tree-level diagrams for the initial state $d\bar{d}$. Analogous diagrams exist for the other down-type quarks, $q = s, b$, and for light up-type quarks, $q = u, c$, while top quarks are not considered as active quarks in the proton at LHC energies. The LO diagrams for $\gamma\gamma$ collisions are, for instance, depicted in figure 1 of ref. [37].

NLO EW corrections, i.e. corrections of $\mathcal{O}(\alpha)$ with respect to LO, comprise purely EW virtual one-loop diagrams and real corrections with one additional external photon. In total, there are $\mathcal{O}(10^3)$ different one-loop diagrams per $\bar{q}q$ channel. In figure 2, we show examples for the most complicated one-loop topology involving six loop propagators (so-called hexagon diagrams).

The real photonic corrections are classified into bremsstrahlung corrections with $\nu_\mu \mu^+ e^- \bar{\nu}_e + \gamma$ final states,
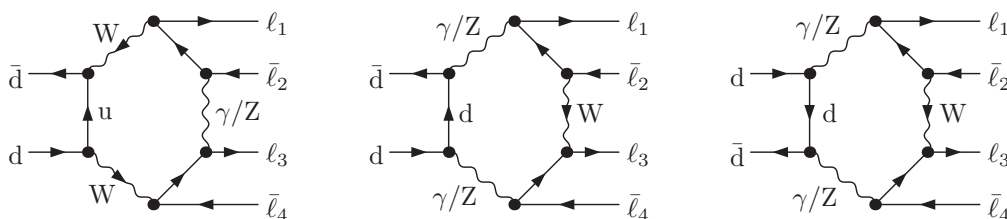
$$\bar{q}q/q\bar{q}/\gamma\gamma \to \nu_\mu \mu^+ e^- \bar{\nu}_e + \gamma, \qquad (2.3)$$

and photon-induced contributions with an additional $q/\bar{q}$ in the final state,

$$q\gamma/\gamma q \to \nu_\mu \mu^+ e^- \bar{\nu}_e + q,$$
$$\bar{q}\gamma/\gamma\bar{q} \to \nu_\mu \mu^+ e^- \bar{\nu}_e + \bar{q}. \qquad (2.4)$$
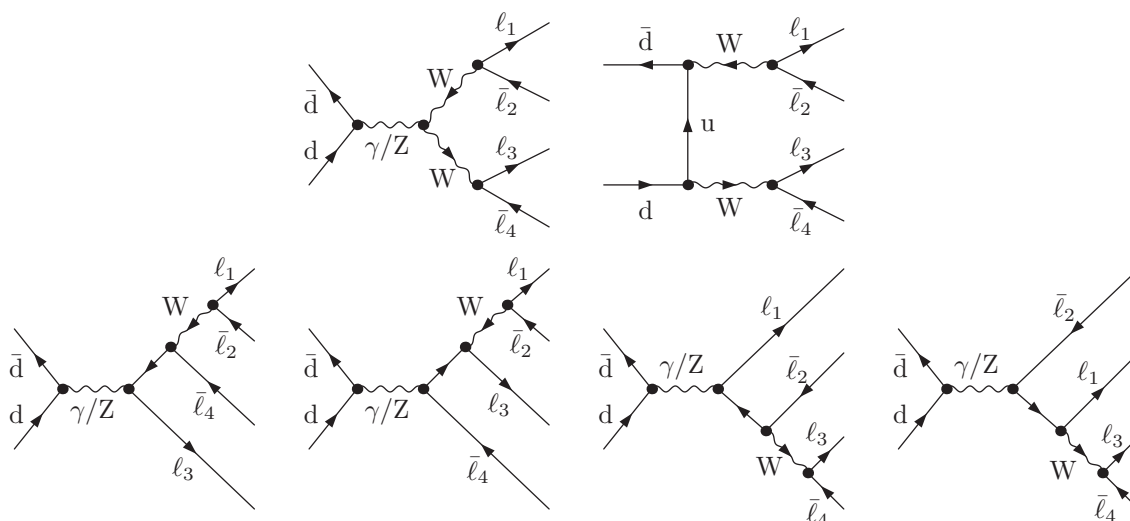
Figure 1. Tree-level diagrams for the partonic (charged-current) process $\bar{\mathrm{d}}\mathrm{d} \to 4$ leptons.

Figure 2. Hexagon diagrams for the partonic (charged-current) process $\bar{\mathrm{d}}\mathrm{d} \to 4$ leptons. The remaining hexagon diagrams are obtained by reversing the fermion flow in one or both of the fermion lines of the outgoing fermions and by exchanging $\ell_1 \leftrightarrow \bar{\ell}_2$ and/or $\ell_3 \leftrightarrow \bar{\ell}_4$.

To simplify our notation in the following, we generically refer to the $q\bar{q}/\bar{q}q$ initial states as $\bar{q}q$, and to the ones in eq. (2.4) as $q\gamma$. Owing to the suppression of the LO $\gamma\gamma$ contribution, NLO corrections to $\gamma\gamma$ collisions can be neglected in predictions for pp cross sections targeting at percent accuracy. Note that the $\mathcal{O}(\alpha)$ corrections to $\gamma\gamma \to \mathrm{WW} \to 4$ leptons are known in DPA [54], without revealing any unexpected enhancements in this channel. We thus base our calculation on the full LO results including all partonic channels of eq. (2.2) and on NLO corrections comprising all virtual EW and real-photonic bremsstrahlung contributions to the antiquark-quark annihilation channels as well as all the $q\gamma$ contributions of eq. (2.4).

We have performed two independent calculations of all contributions and find mutual agreement of the squared amplitudes at individual phase-space points. Cross sections agree within statistical uncertainties of the final Monte Carlo phase-space integration.

The two calculations of the virtual one-loop corrections follow completely independent strategies. One calculation closely follows the approach described in refs. [42, 43], where

NLO EW corrections to $e^+e^- \to 4$ fermions via W-boson pairs were calculated, and builds on ref. [37] for the real corrections and the Monte Carlo integration. In detail, the calculation proceeds diagrammatically, starting with the generation of Feynman diagrams with FEYNARTS [55, 56] and further algebraic processing with in-house MATHEMATICA routines. The other calculation has been carried out with the program RECOLA [48, 49] facilitating the automated generation of NLO EW amplitudes, in combination with an in-house Monte Carlo generator. Additional checks have been performed employing the MATHEMATICA package POLE [57], which internally makes use of FEYNARTS [55, 56] and FORMCALC [58, 59]. The two loop calculations employ different branches of the library COLLIER [50, 51], which is mainly based on the results of ref. [60–62], to evaluate all one-loop integrals with complex W/Z masses with sufficient numerical stability in the four-body phase space.

For the treatment of infrared (soft and/or collinear) singularities, both implementations resort to the dipole subtraction approach, as formulated in refs. [63] and [64] for photon radiation in the cases of collinear-safe and collinear-unsafe observables, respectively. Technically, infrared-singular contributions are treated in dimensional or alternatively in mass regularization, and we have checked numerically that the sum of all (virtual and real) corrections is infrared finite and independent of the regularization scheme. Conceptually, we distinguish between leptons that can be fully isolated from collinear photons and leptons that are recombined with photons in some collinear radiation cone. The former case is only relevant for muons and leads to *collinear-unsafe* observables, which receive mass-singular photonic corrections $\propto (\alpha/\pi) \ln(m_\mu/Q)$, where Q is some hard scale. On the other hand, the recombination of leptons and collinear photons is necessary for a realistic treatment of electrons which are detected as showers in the electromagnetic calorimeter. In this case, the mass-singular corrections are mitigated to corrections that are logarithmically sensitive to the resolution parameter of the recombination cone.

Apart from the algebraic complexity, a major complication in the NLO EW calculation arises from the appearance of resonances which require at least a partial Dyson summation of self-energy corrections to potentially resonant propagators, a procedure that jeopardizes the gauge invariance of the result, if no particular care is taken. We employ the complex-mass scheme [43, 52, 53] which provides a gauge-invariant solution to this problem at NLO by replacing the real W- and Z-boson masses by complex quantities, including also the corresponding complexification of EW couplings. We emphasize that the complex-mass scheme maintains NLO precision everywhere in phase space, i.e. in regions with any number of resonant or non-resonant W bosons.

2.2 Full off-shell calculation versus double-pole approximation

Motivated by the dominance of the doubly-resonant contributions to the cross section of the W-pair production process $pp \to \nu_\mu \mu^+ e^- \bar{\nu}_e + X$, previous calculations of EW corrections were based on on-shell W bosons [34–36, 38] or an expansion about the W resonances [31, 32, 37]. More precisely, the DPA described in ref. [37] employed full matrix elements for all LO contributions and real-photonic corrections and applied the pole expan-
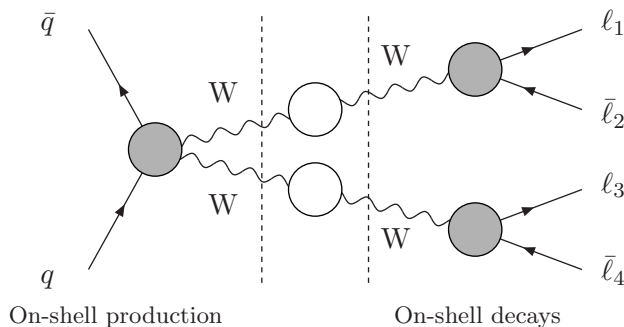
Figure 3. Generic diagram for virtual factorizable corrections to $\bar{q}q \to$ WW $\to 4$ leptons appearing in DPA, where the blobs stand for tree-level or one-loop insertions.
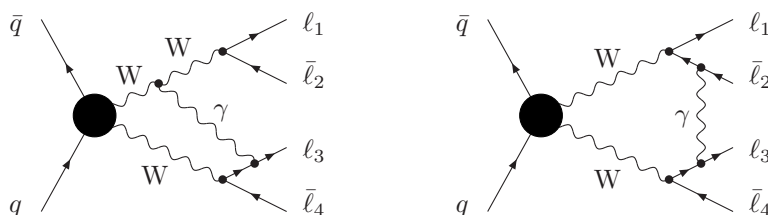
Figure 4. Typical diagrams contributing to the virtual non-factorizable corrections to $\bar{q}q \to$ WW $\to 4$ leptons appearing in DPA, where the blobs stand for any tree-level subdiagram.

sion only to the virtual corrections, following the approach suggested already for $e^+e^- \to$ WW $\to 4f$ at LEP2[1] and implemented in the Monte Carlo generator RACOONWW [44–46].

The DPA for the virtual corrections classifies the doubly-resonant loop contributions into two gauge-invariant categories, known as *factorizable* and *non-factorizable* corrections. The former comprise all corrections that can be attributed to the production or to the decays of the resonances; the corresponding generic diagram for this type is shown in figure 3. The non-factorizable corrections comprise all doubly-resonant contributions that are due to particle exchange between the various production and decay subprocesses. Owing to the fact that only soft-photon exchange (as illustrated in figure 4) leads to doubly-resonant non-factorizable contributions, they take the form of a single correction factor to the lowest-order amplitude. The terminology "non-factorizable" refers to the non-trivial off-shell behaviour of the correction, which is not a simple product of resonance propagators. More details on the DPA, and more general results on pole approximations, can be found in refs. [31, 32, 37, 44–46, 54, 65–67, 69].

In order to prepare our comparison of results based on the full four-fermion $(4f)$ calculation to DPA results, we briefly summarize the most important differences between the two approaches:

- From the practical point of view, the DPA is simpler to work out, since the multiplicities of the underlying loop amplitudes for production and decays are much smaller. In

---

[1]Similar DPA variants for W-pair productions at LEP2 were suggested in refs. [65–67] and compared in ref. [68].

our case, the complexity of the DPA loop calculations is the one of $2 \to 2$ production and $1 \to 2$ decay processes with about $\mathcal{O}(10^2)$ diagrams per partonic channel, and mostly real particle masses. On the other hand, the $2 \to 4$ particle loop calculation involves $\mathcal{O}(10^3)$ diagrams up to hexagon topology with complex internal masses.

As a result of this difference and due to the possibility of an efficient numerical expansion of $2 \to 2$ loop amplitudes into tree-level-like form factors [44–46, 54], the numerical evaluation of the DPA can become almost comparable in speed to a tree-level calculation, while the full $4f$ calculation is CPU intensive.

- The strength of the full off-shell $4f$ calculation rests in its NLO accuracy everywhere in phase space, i.e. the intrinsic perturbative uncertainty Δ_{4f} of this approach is generically given by the size of the higher-order corrections that are not yet calculated. For the purely EW corrections, we thus expect $\Delta_{4f} \sim \delta_{\mathrm{EW}}^2$ if δ_{EW} is the relative NLO EW correction factor.

By contrast, the validity of the DPA is restricted to regions in phase space where the double resonance of the W-boson pair dominates the cross section. Taken literally, this restricts the DPA to four-lepton final states with invariant masses $M_{4\ell} > 2M_{\mathrm{W}} + n\Gamma_{\mathrm{W}}$ and $|M_{\ell_i \bar{\nu}_i} - M_{\mathrm{W}}| \lesssim n\Gamma_{\mathrm{W}}$, where $n \sim 2\text{–}3$ is some small number and $\ell_i \bar{\nu}_i$ generically stands for the two lepton-neutrino pairs from the W-boson decays. To extend the calculation of EW corrections below the W-pair threshold at $M_{4\ell} = 2M_{\mathrm{W}}$, an *improved Born approximation* based on the leading universal corrections is used for $M_{4\ell} < 2M_{\mathrm{W}} + n\Gamma_{\mathrm{W}}$. In practice, the DPA is applicable if contributions from regions below the W-pair threshold and off-shell regions are sufficiently suppressed.

The theoretical uncertainty Δ_{DPA} of the DPA thus is not only given by the typical size of missing higher-order corrections, but also set by the intrinsic uncertainty of the pole expansion. Assuming that all LO contributions are based on full matrix elements and that the relative correction in DPA, $\delta_{\mathrm{EW}}^{\mathrm{DPA}}$, is normalized to the full LO cross section σ_{LO}, i.e.

$$\sigma_{\mathrm{NLO\,EW}}^{\mathrm{DPA}} = \sigma_{\mathrm{LO}} + \Delta\sigma_{\mathrm{EW}}^{\mathrm{DPA}} = \sigma_{\mathrm{LO}} \left(1 + \delta_{\mathrm{EW}}^{\mathrm{DPA}}\right), \qquad \delta_{\mathrm{EW}}^{\mathrm{DPA}} = \frac{\Delta\sigma_{\mathrm{EW}}^{\mathrm{DPA}}}{\sigma_{\mathrm{LO}}}, \qquad (2.5)$$

we estimate Δ_{DPA} to

$$\Delta_{\mathrm{DPA}} \sim \max\left\{ \left(\delta_{\mathrm{EW}}^{\mathrm{DPA}}\right)^2, \underbrace{\frac{\alpha}{\pi} \frac{\Gamma_{\mathrm{W}}}{M_{\mathrm{W}}} \ln(\ldots)}_{\lesssim\, 0.5\%}, \left|\delta_{\mathrm{EW}}^{\mathrm{DPA}}\right| \times \frac{|\sigma_{\mathrm{LO}} - \sigma_{\mathrm{LO}}^{\mathrm{DPA}}|}{\sigma_{\mathrm{LO}}^{\mathrm{DPA}}} \right\}. \qquad (2.6)$$

The first term on the r.h.s. of eq. (2.6) corresponds to the missing higher-order EW corrections, similar to the NLO limitation of Δ_{4f}. The second term indicates the size of the off-shell contributions to the EW corrections in regions where the DPA applies. This estimate is based on the typical size of the respective effects: the off-shell contributions amounting to a fraction $\sim \Gamma_{\mathrm{W}}/M_{\mathrm{W}}$, and the EW corrections being of order $\sim \alpha/\pi$ times some moderate logarithmic factor (see also refs. [37, 42–46]).

The last term on the r.h.s. of eq. (2.6) mimics the failure of the DPA upon blowing up the relative correction $\delta_{\mathrm{EW}}^{\mathrm{DPA}}$ by the factor $|\sigma_{\mathrm{LO}} - \sigma_{\mathrm{LO}}^{\mathrm{DPA}}|/\sigma_{\mathrm{LO}}^{\mathrm{DPA}}$ that is deduced from the LO cross sections based on the full $4f$ or DPA matrix elements.[2] As we will see below, the last term in Δ_{DPA} is surprisingly large in some transverse-momentum distributions in the TeV range.

3 Phenomenological results

3.1 Input parameters and calculational setup

For our numerical studies we consider proton-proton collisions at the LHC at centre-of-mass energies of $\sqrt{s_{\mathrm{pp}}} = 8\,\mathrm{TeV}$ and $13\,\mathrm{TeV}$. We use the SM input parameters

$$
\begin{aligned}
G_\mu &= 1.1663787 \times 10^{-5}\,\mathrm{GeV}^{-2}, & \alpha(0) &= 1/137.035999, \\
M_{\mathrm{W}}^{\mathrm{OS}} &= 80.385\,\mathrm{GeV}, & \Gamma_{\mathrm{W}}^{\mathrm{OS}} &= 2.085\,\mathrm{GeV}, \\
M_{\mathrm{Z}}^{\mathrm{OS}} &= 91.1876\,\mathrm{GeV}, & \Gamma_{\mathrm{Z}}^{\mathrm{OS}} &= 2.4952\,\mathrm{GeV}, \\
M_{\mathrm{H}} &= 125.9\,\mathrm{GeV}, & m_\mu &= 0.1057\,\mathrm{GeV}, \\
m_{\mathrm{t}} &= 173.07\,\mathrm{GeV}, & \Gamma_{\mathrm{t}} &= 2\,\mathrm{GeV},
\end{aligned} \tag{3.1}
$$

following ref. [70]. The muon mass m_μ is only relevant in the case of a collinear-unsafe treatment of collinear photon emission off final-state muons, otherwise all fermions except for the top quark are considered as massless. The finite width of the top quark is only used in the contributions from $b\gamma$ initial states, as discussed below.

Throughout, we apply the complex-mass scheme for the W and Z resonances, employing complex vector-boson masses μ_{V} defined by

$$
\mu_{\mathrm{V}}^2 = M_{\mathrm{V}}^2 - \mathrm{i}M_{\mathrm{V}}\Gamma_{\mathrm{V}}, \qquad \mathrm{V} = \mathrm{W}, \mathrm{Z}, \tag{3.2}
$$

with the real mass values M_{V} and constant vector-boson decay widths Γ_{V}. In this scheme, the weak mixing angle θ_{w} governing the coupling structure of the EW sector is computed from the complex masses,

$$
\cos\theta_{\mathrm{w}} \equiv c_{\mathrm{w}} = \sqrt{1 - s_{\mathrm{w}}^2} = \mu_{\mathrm{W}}/\mu_{\mathrm{Z}}, \tag{3.3}
$$

and therefore enters the calculation as a complex quantity. However, the gauge-boson mass and width values given in eq. (3.1) correspond to the "on-shell" (OS) masses and widths, which were measured at LEP and the Tevatron using a running-width prescription. Consequently, we convert these OS values $M_{\mathrm{V}}^{\mathrm{OS}}$ and $\Gamma_{\mathrm{V}}^{\mathrm{OS}}$ ($\mathrm{V} = \mathrm{W}, \mathrm{Z}$) to the "pole values" denoted by M_{V} and Γ_{V} according to [71],

$$
M_{\mathrm{V}} = M_{\mathrm{V}}^{\mathrm{OS}}/\sqrt{1 + (\Gamma_{\mathrm{V}}^{\mathrm{OS}}/M_{\mathrm{V}}^{\mathrm{OS}})^2}, \qquad \Gamma_{\mathrm{V}} = \Gamma_{\mathrm{V}}^{\mathrm{OS}}/\sqrt{1 + (\Gamma_{\mathrm{V}}^{\mathrm{OS}}/M_{\mathrm{V}}^{\mathrm{OS}})^2}, \tag{3.4}
$$

---

[2]The last uncertainty factor in eq. (2.6) can also be written as $\Delta\sigma_{\mathrm{EW}}^{\mathrm{DPA}}/\sigma_{\mathrm{LO}}^{\mathrm{DPA}} \times |\sigma_{\mathrm{LO}} - \sigma_{\mathrm{LO}}^{\mathrm{DPA}}|/\sigma_{\mathrm{LO}}$, where $\Delta\sigma_{\mathrm{EW}}^{\mathrm{DPA}}/\sigma_{\mathrm{LO}}^{\mathrm{DPA}}$ would then be interpreted as the intrinsic relative EW correction of the DPA and $|\sigma_{\mathrm{LO}} - \sigma_{\mathrm{LO}}^{\mathrm{DPA}}|/\sigma_{\mathrm{LO}}$ is the relative deviation of the DPA LO from the full $4f$ LO cross section. However, we chose the form of eq. (2.6) to be compatible with the definition of $\delta_{\mathrm{EW}}^{\mathrm{DPA}}$ made in ref. [37] and the earlier e^+e^- references such as ref. [42].

leading to

$$M_{\mathrm{W}} = 80.357\ldots\,\mathrm{GeV}, \qquad \Gamma_{\mathrm{W}} = 2.0842\ldots\,\mathrm{GeV},$$
$$M_{\mathrm{Z}} = 91.153\ldots\,\mathrm{GeV}, \qquad \Gamma_{\mathrm{Z}} = 2.4942\ldots\,\mathrm{GeV}. \tag{3.5}$$

Although the difference between using $M_{\mathrm{V}}^{\mathrm{OS}}$ and M_{V} would be hardly visible in phenomenological results, we use the latter as input for our numerics.

In the $\bar{q}q$-induced contributions we determine all couplings in the G_μ scheme, where α is defined in terms of the input parameters given in eqs. (3.1) and (3.5),

$$\alpha_{G_\mu} = \frac{\sqrt{2}\,G_\mu M_{\mathrm{W}}^2}{\pi} \left(1 - \frac{M_{\mathrm{W}}^2}{M_{\mathrm{Z}}^2} \right). \tag{3.6}$$

This setting minimizes universal weak corrections beyond NLO in the high-energy tails of distributions where high-energy logarithms due to soft/collinear W/Z bosons dominate the EW corrections. However, we set $\alpha = \alpha(0)$ for the couplings of the incoming photons in the photon-induced ($q\gamma$ and $\gamma\gamma$) channels, since $\alpha(0)$ is the relevant electromagnetic coupling for real (external) photons. Therefore, the squared matrix elements for $q\gamma \to 2\ell 2\nu + q$ and $\gamma\gamma \to 2\ell 2\nu$ scale like $\alpha(0)\alpha_{G_\mu}^4$ and $\alpha(0)^2\alpha_{G_\mu}^2$, respectively.

The CKM matrix is set to the unit matrix throughout, without restricting the validity of our calculation. In fact, since mixing to the third quark generation is phenomenologically negligible and since we work with mass-degenerate (massless) light quark generations, the CKM matrix disappears from all amplitudes via its unitarity relations after summing over intermediate quark states.

For the calculation of the hadronic cross section, we use the $\mathcal{O}(\alpha)$-corrected PDF set NNPDF2.3QED [41], which also includes a distribution function for the photon. Since the considered LO cross section and the EW corrections do not depend on the strong coupling, all our results exhibit a very weak scale dependence. We therefore see no benefit in introducing a specific dynamical scale, but choose a fixed factorization and renormalization scale setting

$$\mu_{\mathrm{F}} = \mu_{\mathrm{R}} = M_{\mathrm{W}}, \tag{3.7}$$

as the default. Following the arguments of ref. [72], we employ a DIS-like factorization scheme for the QED corrections because EW corrections are not taken into account in the fit of the PDFs to data.

In subprocesses with a final-state quark or antiquark, a parton i is only considered as jet if its transverse momentum $p_{\mathrm{T},i}$ and its rapidity $|y_i|$ allow for a proper detection in experiment. For a parton i we require

$$p_{\mathrm{T},i} > p_{\mathrm{T,jet}}^{\mathrm{def}} = 25\,\mathrm{GeV}, \qquad |y_i| < |y_{\mathrm{jet}}^{\mathrm{def}}| = 5, \tag{3.8}$$

for being treated as a jet. If the parton does not meet these two requirements, it is treated as *invisible jet*, which means that no additional jet-related cuts are applied and its momentum contributes to $\vec{p}_{\mathrm{T}}^{\,\mathrm{miss}}$. A similar treatment is applied to final-state photons with rapidities outside the range accessible to the detector, which therefore remain undetected. We consider final-state photons with

$$|y_\gamma| > 5, \tag{3.9}$$

as *invisible photons*, and the corresponding momentum is part of the missing momentum.

As mentioned above, we provide two different setups concerning the treatment of nearly collinear photons: in the *collinear-safe setup*, nearly collinear photons are recombined with both final-state electrons and muons, whereas in the *collinear-unsafe setup*, we apply the photon recombination procedure only to final-state electrons while photons are never recombined with muons. The applied recombination procedure mimics the experimental concept of "dressed leptons" used by ATLAS (see e.g. ref. [73]), which avoids the experimental problem to separately resolve an electron and a nearly collinear photon. As measure for the collinearity of photons and leptons, their distance R_{ij} in the rapidity-azimuthal-angle plane is used, where

$$R_{ij} = \sqrt{(y_i - y_j)^2 + \Delta\phi_{ij}^2} \tag{3.10}$$

with $y_{i,j}$ denoting the rapidities of particle i and j and $\Delta\phi_{ij}$ their azimuthal angle difference, respectively. Whenever the separation is smaller than

$$R_{\gamma\ell}^{\mathrm{recomb}} = 0.1, \tag{3.11}$$

we add the photon momentum to the respective lepton and discard the photon from the event, while the momenta of all other particles in the event remain unaffected.

3.2 Event selection

We compare results for three different event-selection setups: (i) defined by basic particle identification only ("inclusive setup"), (ii) designed by ATLAS for enhancing the WW signal ("ATLAS WW setup"), and (iii) inspired by Higgs-boson analyses in the decay channel $H \to WW^*$ ("Higgs-background setup"), where direct W-pair production appears as irreducible background. For the latter two setups we present results for integrated and differential cross sections, for the inclusive setup we show integrated results only.

(i) Inclusive setup. After a potential photon recombination we define the events for the process $pp \to \nu_\mu \mu^+ e^- \bar{\nu}_e + X$ by requiring the μ^+ and e^- to have transverse momenta

$$p_{\mathrm{T},\ell} > 20\,\mathrm{GeV}, \tag{3.12}$$

in the central rapidity region of the detector,

$$|y_\ell| < 2.5. \tag{3.13}$$

For final states with an identified jet (cf. eq. (3.8)) we demand this jet to be well separated from the lepton system, by rejecting any event with

$$R_{\mathrm{jet},\ell} < 0.4. \tag{3.14}$$

In order to suppress overwhelmingly large QCD corrections from additional jet radiation, we employ a jet veto, i.e. we reject any event with

$$p_{\mathrm{T},\mathrm{jet}} > 100\,\mathrm{GeV}. \tag{3.15}$$

(ii) ATLAS WW setup. Moreover, we consider an event selection that is inspired by the analyses of the 7 TeV dataset for pp $\to$ W$^+$W$^-$ + X performed by the ATLAS collaboration [1, 2]. In addition to the afore-mentioned lepton cuts we impose a stronger transverse-momentum cut on the hardest charged lepton and require the two charged leptons to be well separated from each other by imposing the cuts

$$p_{\mathrm{T},\ell}^{\mathrm{leading}} > 25\,\mathrm{GeV}, \qquad R_{\mathrm{e}^-\mu^+} > 0.1, \qquad M_{\mathrm{e}^-\mu^+} > 10\,\mathrm{GeV}. \tag{3.16}$$

For a cleaner signature we further demand a non-vanishing missing transverse momentum,

$$E_{\mathrm{T}}^{\mathrm{miss}} = |\vec{p}_{\mathrm{T}}^{\,\mathrm{miss}}| > 25\,\mathrm{GeV}, \tag{3.17}$$

and remind the reader that invisible jets and invisible photons do also enter this quantity. To further suppress the influence of QCD corrections, we veto all events with hard final-state jets obeying

$$p_{\mathrm{T,jet}} > 25\,\mathrm{GeV}. \tag{3.18}$$

Note that according to eq. (3.8), all events with a detected jet are discarded due to this cut.

(iii) Higgs-background setup. Inspired by the recent analyses of the decay of the Higgs boson to WW* independently performed by ATLAS [74] and CMS [75] we study the influence of EW corrections on the main irreducible background, namely pp $\to$ WW$^* \to \nu_\mu\mu^+\mathrm{e}^-\bar{\nu}_\mathrm{e} + X$, in a realistic cut scenario. Essentially following ref. [74], we extend the ATLAS WW setup of eqs. (3.16)–(3.18) by two additional cuts,

$$10\,\mathrm{GeV} < M_{\mathrm{e}^-\mu^+} < 55\,\mathrm{GeV}, \qquad \Delta\phi_{\mathrm{e}^-\mu^+} < 1.8, \tag{3.19}$$

which are designed to favour the signal topology of the H$\to$ WW* analysis and therefore significantly suppress direct WW* production. Additionally, we adjust the threshold of the transverse-momentum cut to the value used in the experimental analysis,

$$E_{\mathrm{T}}^{\mathrm{miss}} = |\vec{p}_{\mathrm{T}}^{\,\mathrm{miss}}| > 20\,\mathrm{GeV}. \tag{3.20}$$

3.3 Results on integrated cross sections

In table 1 we present the quark-initiated LO cross sections, $\sigma_{\bar{q}q}^{\mathrm{LO}}$, for pp $\to \nu_\mu\mu^+\mathrm{e}^-\bar{\nu}_\mathrm{e}+X$ at the LHC for the energies $\sqrt{s_{\mathrm{pp}}} = 8\,\mathrm{TeV}$ and $\sqrt{s_{\mathrm{pp}}} = 13\,\mathrm{TeV}$ within the three different setups defined in section 3.2. The numbers include the five $\bar{q}q$-initiated contributions induced by the light quarks. Due to the small bottom-quark PDFs, the $\bar{\mathrm{b}}\mathrm{b}$ channel comprises less than 2% of the LO cross section in all considered setups. The LO $\gamma\gamma$-induced subprocess gives rise to a (sub-)percent correction to $\sigma_{\bar{q}q}^{\mathrm{LO}}$, so that we treat $\delta_{\gamma\gamma} = \sigma_{\gamma\gamma}^{\mathrm{LO}}/\sigma_{\bar{q}q}^{\mathrm{LO}}$ as part of the EW corrections.

The NLO corrections of $\mathcal{O}(\alpha)$ consist of virtual one-loop and photonic real-emission contributions to the $\bar{q}q$-induced processes, as well as additional $q\gamma$-, bγ-, and $\gamma\gamma$-initiated tree-level subprocesses. Similarly to the situation at LO, the corrections stemming from subprocesses with initial-state bottom-quark pairs account for less than 2% of the full NLO

LHC		$\sigma_{\bar{q}q}^{\mathrm{LO}}$ [fb]	$\delta_{\bar{q}q}^{\mathrm{NLO}}$ [%]	$\delta_{q\gamma}^{q\neq\mathrm{b}}$ [%]	$\delta_{\gamma\gamma}$ [%]	δ_{EW} [%]	$\delta_{\mathrm{b}\gamma}$ [%]
Inclusive	8 TeV	238.65(3)	-3.28	0.44	0.84	-2.01	1.81
	13 TeV	390.59(3)	-3.41	0.49	0.73	-2.20	2.30
ATLAS WW	8 TeV	165.24(1)	-3.56	-0.26	1.01	-2.81	0.18
	13 TeV	271.63(1)	-3.71	-0.27	0.87	-3.11	0.23
Higgs bkg	8 TeV	31.59(2)	-2.52	-0.21	0.60	-2.13	0.15
	13 TeV	49.934(2)	-2.54	-0.22	0.52	-2.25	0.18

Table 1.   LO cross sections and relative EW corrections to pp $\to \nu_\mu \mu^+ \mathrm{e}^- \bar{\nu}_\mathrm{e} + X$ at the LHC at 8 TeV and 13 TeV, in the inclusive setup (top), the ATLAS WW setup (middle), and the Higgs-background setup (bottom). The numbers in parentheses represent the Monte Carlo uncertainty on the last given digit.

correction. For this reason it is justified to approximate the matrix elements with external bottom quarks in the $\bar{q}q$ contributions by those with massless down quarks (and internal massless up-type weak isospin partner) in the EW corrections, without any notable loss in precision. We follow this approach in our diagrammatic loop calculation, while the second calculation with RECOLA does not make use of this approximation.[3] As default setup for the photonic real-emission contributions we choose the collinear-unsafe setup, as defined in section 3.1. The difference to the collinear-safe setup is discussed in detail in section 3.6 below.

The omission of virtual and photonic real-emission corrections of $\mathcal{O}(\alpha)$ to the $\gamma\gamma$-induced contributions is justified by their small size already at LO. While we include the $\bar{\mathrm{b}}\mathrm{b}$-induced processes in $\bar{q}q$, we display the bγ-initiated contributions separately from $q\gamma$ (containing $q = \mathrm{u}, \mathrm{d}, \mathrm{s}, \mathrm{c}$) as these are the only contributions with bottom quarks in the final state. Note further that the bγ-induced contributions are enhanced by the presence of a top resonance, in particular for the inclusive setup where they reach 2.3%. In the ATLAS WW setup and the Higgs-background setup the contributions of this resonance are suppressed by the jet veto of eq. (3.18). In the following results on differential distributions for the latter two setups we do not include these contributions, which could be further suppressed by a b-jet veto, i.e. we identify $\delta_{q\gamma} \equiv \delta_{q\gamma}^{q\neq\mathrm{b}}$.

In table 1, besides the LO cross sections, we list the relative contributions of the different types of corrections normalized to $\sigma_{\bar{q}q}^{\mathrm{LO}}$. The generally negative $\mathcal{O}(\alpha)$ corrections ($\delta_{\bar{q}q}^{\mathrm{NLO}}$ and $\delta_{q\gamma}$) are somewhat reduced by the positive LO $\gamma\gamma$ correction, so that their sum (δ_{EW}) leads to a small negative correction of roughly $-(2\text{–}3)\%$ on the integrated cross section for all investigated setups. However, as well known from previous studies of W-boson pair production at hadron colliders [31–37], the EW corrections become very important in differential distributions where they lead to significant distortions.

---

[3]In all considered setups, we find the difference on $\delta_{\bar{q}q}^{\mathrm{NLO}}$ to be below 0.02% between the two approaches. The numbers in table 1 are obtained in the approximation where the top quark is treated as massless.

3.4 Results on differential cross sections in the ATLAS WW setup

In this section we inspect some important differential cross sections evaluated in the ATLAS WW setup for the collinear-unsafe photon scenario. Here and in the following sections, we show, for an LHC energy of $\sqrt{s_{\mathrm{pp}}} = 13\,\mathrm{TeV}$, absolute predictions for $\mathrm{d}\sigma/\mathrm{d}\mathcal{O}$ as histograms binned in the observable $\mathcal{O}$ in the upper panel, followed by the relative corrections of type i,

$$\delta_i(\mathcal{O}) = \frac{\mathrm{d}\sigma^i}{\mathrm{d}\mathcal{O}} \Big/ \frac{\mathrm{d}\sigma_{\bar{q}q}^{\mathrm{LO}}}{\mathrm{d}\mathcal{O}}, \tag{3.21}$$

directly below.

In figure 5, we display the transverse-momentum distribution of the electron. We first concentrate on the left-hand side (l.h.s.) of the figure. In the upper panel, LO refers to $\sigma_{\bar{q}q}^{\mathrm{LO}}$ induced by $\bar{q}q$ channels only, $\gamma\gamma$ to $\sigma_{\gamma\gamma}^{\mathrm{LO}}$ induced by photon-photon collisions, and EW to the full NLO EW prediction, i.e. the sum of the LO cross section with all considered corrections. The $\bar{b}b$-induced contribution to $\sigma_{\bar{q}q}^{\mathrm{LO}}$ (not shown separately) is only relevant at low p_{T,e^-}, dropping below 2% already at $p_{\mathrm{T},e^-} \sim 300\,\mathrm{GeV}$. The lower panel compares the relative corrections induced by the $\bar{q}q$, $q\gamma$, and $\gamma\gamma$ channels as well as their sum (EW). The corrections in the $\bar{q}q$ channels dominate and exhibit their known negative logarithmic increase due to weak Sudakov (and subleading) high-energy logarithms $\propto \alpha/(\pi s_{\mathrm{w}}^2)\ln^2(p_{\mathrm{T},e^-}/M_{\mathrm{W}})$, reaching $\sim -45\%$ at $p_{\mathrm{T},e^-} = 1\,\mathrm{TeV}$. This huge negative correction is only partly compensated by the positive contribution of the $\gamma\gamma$-induced tree-level process, whose impact steadily grows from about 1% at small transverse momentum to more than 10% at 1 TeV. The contribution of the $q\gamma$-induced channel is completely insignificant within the ATLAS WW setup.

The behaviour of the $q\gamma$ contribution is enforced by the jet-identification criterion and the specific choice of the jet veto within the ATLAS WW setup, eqs. (3.8) and (3.18), respectively. Both only affect the $q\gamma$-induced contribution, since it is the only contribution that can give rise to a jet. On the right-hand side (r.h.s.) of figure 5 we illustrate the dependence on the jet veto (JV) by means of the transverse-momentum distribution of the electron, where we show the $q\gamma$-induced contribution together with the full EW correction for three different values of the jet veto. If we loosen the cut of eq. (3.18) to only reject jets with $p_{\mathrm{T,jet}} > 100\,\mathrm{GeV}$ (the value within our inclusive setup, eq. (3.15)), the $q\gamma$-induced contribution becomes positive and leads to a correction of +0.62% for the integrated cross section, resembling the situation in the inclusive setup. However, the complete omission of a jet veto results in a positive correction of almost 70% at $p_{\mathrm{T},e^-} = 1\,\mathrm{TeV}$, even rendering the total EW correction δ_{EW} positive for $p_{\mathrm{T},e^-} \gtrsim 400\,\mathrm{GeV}$. In the latter case we obtain a positive correction of $\sigma_{q\gamma} = 3.914(2)\,\mathrm{fb}$ ($\delta_{q\gamma} = +1.44\%$) to the integrated cross section from the $q\gamma$ channel alone, leading to a total EW correction of only $\delta_{\mathrm{EW}} = -1.40\%$. The reason for this immense increase is a known mechanism, referred to as "giant K factor" [76], which was already discussed for $q\gamma$-induced corrections to W-pair production in the literature [36, 37]. In such processes, topologies that first occur at NLO introduce kinematic configurations in which one massive gauge boson may become quasi-soft, leading to large double-logarithmic corrections for large transverse momenta. In QCD, such corrections may grow to several 100%. For $q\gamma$ collisions the size is mitigated by the smallness of α
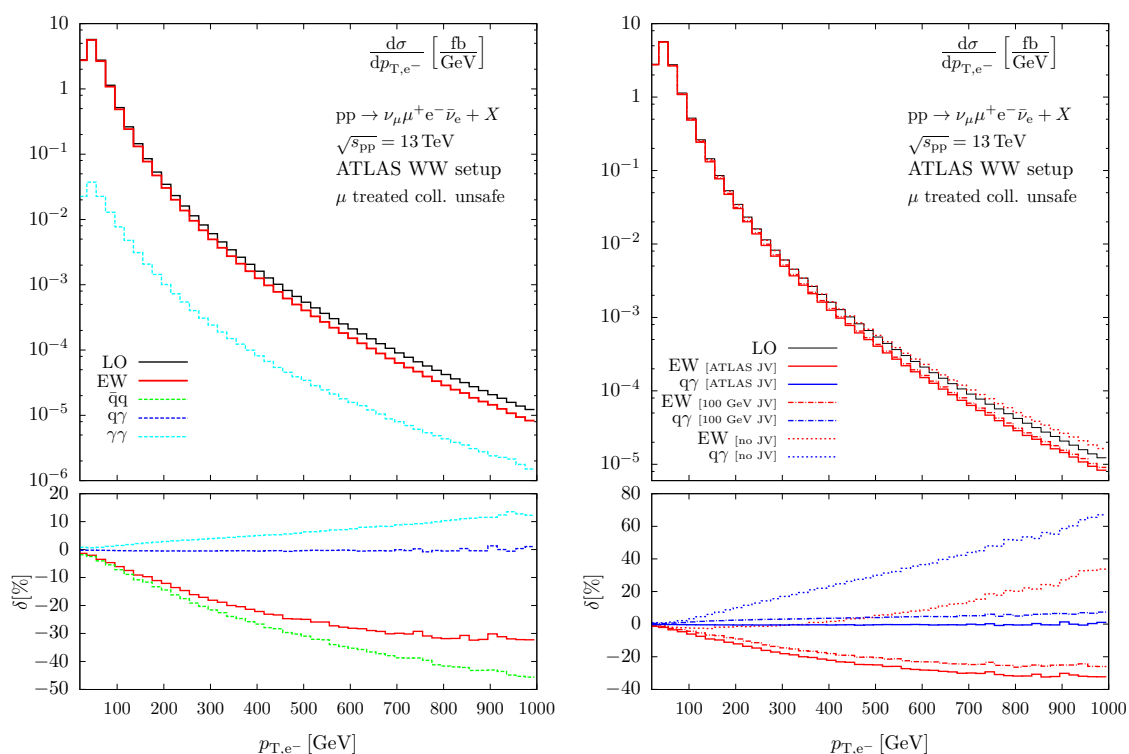
Figure 5. Individual contributions to the differential cross section with the default ATLAS jet veto of $p_{\mathrm{T,jet}} > 25\,\mathrm{GeV}$ (left) and jet-veto (JV) dependence (right) of the transverse-momentum distribution of the electron in $\mathrm{pp} \to \nu_\mu \mu^+ \mathrm{e}^- \bar{\nu}_\mathrm{e} + X$ in the ATLAS WW setup. The lower panels show the relative size of the various corrections.

and the photon PDF with respect to α_s and the gluon PDF, respectively, in spite of some enhancement due to diagrams with incoming photons coupling to W bosons, which do not have a QCD counterpart. Note also that overwhelmingly large QCD corrections (as a consequence of a missing jet veto) would force us to calculate EW corrections for W-pair production in association with hard jets, a task that goes beyond the scope of this paper.

In the following we always apply the jet veto in order to suppress configurations with hard jets and soft W bosons, which are less interesting for the investigation of W-boson pairs. For the ATLAS WW and Higgs-background setups, the jet veto actually implies that $q\gamma$-induced events may only contribute to the zero-jet cross section, so that any potential final-state jet must remain undetected (cf. eq. (3.8)). This eventually leads to a small negative contribution of the $q\gamma$-induced processes in the ATLAS WW setup of $\sigma_{q\gamma} = -0.744(2)\,\mathrm{fb}$ ($\delta_{q\gamma} = -0.27\%$), the value quoted in table 1.

In figure 6 we turn to distributions in the transverse invariant masses of four or two leptons. Owing to the incomplete information about the momenta of the two neutrinos at a hadron collider, it is experimentally not possible to fully reconstruct the invariant mass of the $\mathrm{W^+W^-}$ system (M_{WW}) in leptonic final states. However, in the transverse plane the sum of the neutrino momenta can be inferred from the missing transverse momentum
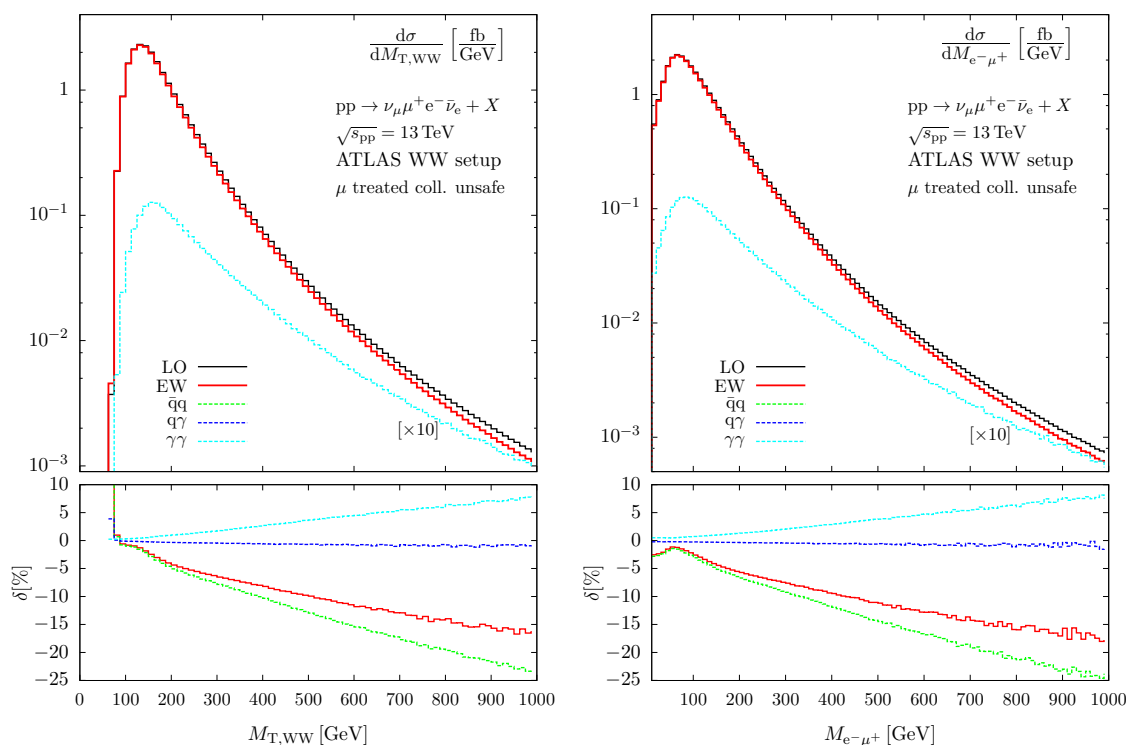
Figure 6. Transverse-mass distribution of the four-lepton system (left) and invariant-mass distribution of the charged-lepton system (right) in pp $\to \nu_\mu \mu^+ e^- \bar{\nu}_e + X$ in the ATLAS WW setup (upper panels), together with the relative impact of the individual corrections (lower panels). Note that the $\gamma\gamma$ contribution is scaled by a factor of ten only in the upper panels.

$(\vec{p}_T^{\,\mathrm{miss}})$, motivating the following definition of the transverse mass of the four-lepton decay system [77],

$$M_{\mathrm{T,WW}} = \sqrt{(E_{\mathrm{T,e^-\mu^+}} + E_T^{\mathrm{miss}})^2 - (\vec{p}_{\mathrm{T,e^-\mu^+}} + \vec{p}_T^{\,\mathrm{miss}})^2}, \qquad (3.22)$$

with the vector sum $\vec{p}_{\mathrm{T,e^-\mu^+}}$ of the transverse momenta of the final-state charged leptons, the missing transverse momentum $\vec{p}_T^{\,\mathrm{miss}}$ and the corresponding transverse energies given by

$$E_{\mathrm{T,e^-\mu^+}} = \sqrt{(\vec{p}_{\mathrm{T,e^-\mu^+}})^2 + M_{e^-\mu^+}^2} \quad \text{and} \quad E_T^{\mathrm{miss}} = |\vec{p}_T^{\,\mathrm{miss}}|. \qquad (3.23)$$

The various contributions to the observable $M_{\mathrm{T,WW}}$ are shown in figure 6 (l.h.s.) together with the invariant mass $M_{e^-\mu^+}$ of the charged-lepton system (r.h.s.). In the high-energy regions, the relative corrections to the two observables exhibit a very similar quantitative behaviour: as for the transverse momentum of the electron, the EW correction is dominated by the negative correction to the $\bar{q}q$-induced processes. The positive contribution of the $\gamma\gamma$-induced tree-level process partly compensates for the strong negative correction, while the contribution from $q\gamma$ initial states remains insignificant due to the jet veto. At the scale of $1\,\mathrm{TeV}$, we observe a negative total EW correction of about -15% for both observables, i.e. about half the size as in the $p_{\mathrm{T,e^-}}$ distribution at the same scale. Note, however, that
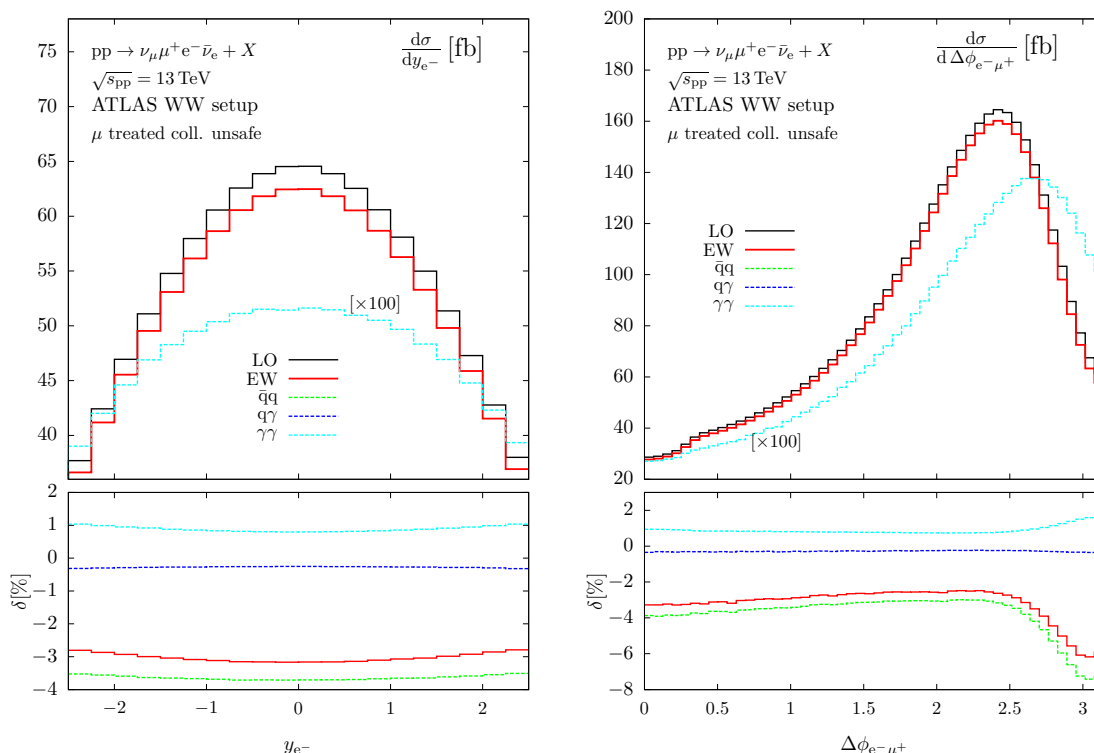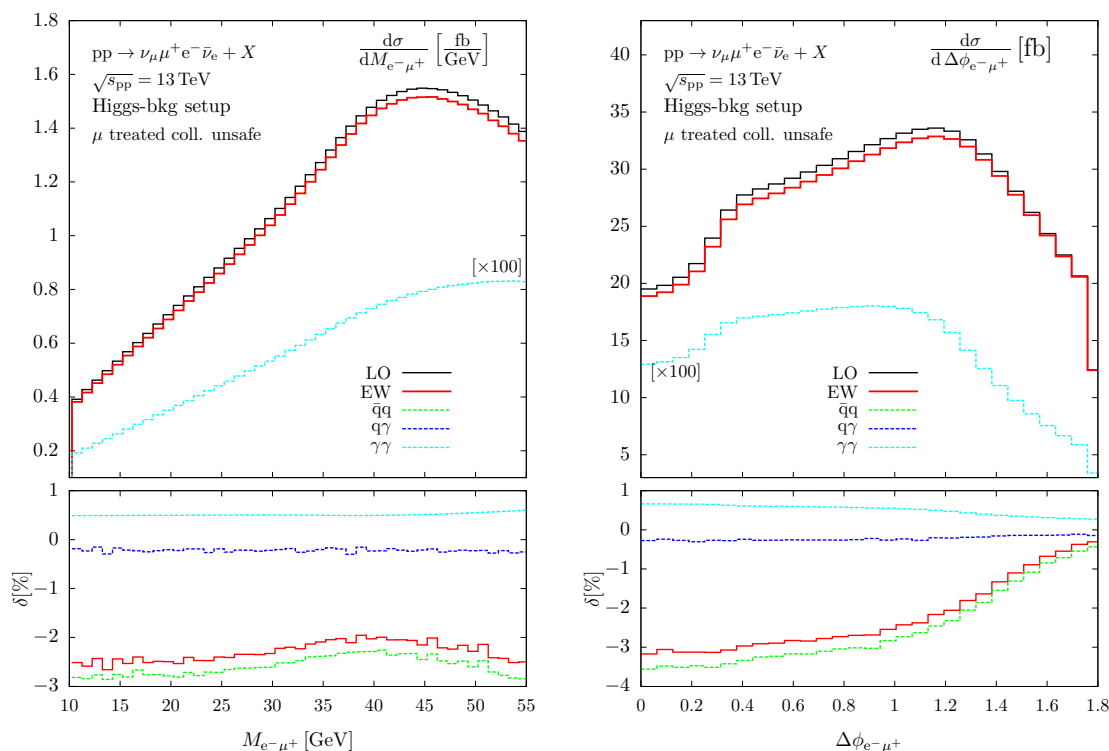
Figure 7. Rapidity distribution of the electron (left) and distribution in the azimuthal-angle separation of the two charged leptons (right) in pp → $\nu_\mu\mu^+e^-\bar{\nu}_e + X$ in the ATLAS WW setup. The lower panels show the relative impact of the various contributions. Note that the $\gamma\gamma$ contribution is scaled by a factor of hundred only in the upper panels.

$\mathrm{d}\sigma/\mathrm{d}p_{\mathrm{T},e^-}$ falls off much steeper with p_{T,e^-} than the shown invariant-mass distributions with increasing masses.

In figure 7 we show rapidity and angular distributions of the charged leptons within the ATLAS WW setup. The corrections to the rapidity distribution of the electron (left) are uniformly distributed and resemble the corrections to the integrated cross sections given in table 1. The azimuthal-angle separation of the two charged leptons (right), on the other hand, receive some distortion due to the EW corrections towards a separation of $\Delta\phi_{e^-\mu^+} = \pi$ of the two charged leptons. This back-to-back configuration in the transverse plane is favoured by events with W-boson pairs with large transverse momenta, which explains the tendency to receive more negative EW corrections in the $\bar{q}q$ channels.

3.5 Results on differential cross sections in the Higgs-background setup

A very important irreducible background to the decay of a Higgs boson to a W-boson pair, H → WW*, originates from the direct W-pair production process pp → WW* → $\nu_\mu\mu^+e^-\bar{\nu}_e + X$. In the following, we study the influence of the EW corrections on this dominant background in the Higgs signal region defined by the additional cuts of eq. (3.19) and eq. (3.20). Since this setup is meant to favour the Higgs signal and to suppress any

Figure 8. Distributions in the invariant mass of the charged-lepton system (left) and in the azimuthal-angle separation of the two charged leptons (right) in pp → $\nu_\mu \mu^+ e^- \bar{\nu}_e + X$ in the Higgs-background setup. The lower panels show the relative impact of the various contributions. Note that the $\gamma\gamma$ contribution is scaled by a factor of hundred only in the upper panels.

background as much as possible, we observe a reduction of $\sigma_{\bar{q}q}^{\mathrm{LO}}$ by almost a factor of six compared to the ATLAS WW setup (cf. table 1). We also observe some reduction of all relative corrections, resulting in a total EW correction of only -2.25% for the 13 TeV prediction (we again provide results for 13 TeV and the collinear-unsafe photon scenario). This reduction can be explained by looking at the differential distributions of the two observables to which the cuts of eq. (3.19) are applied.

In figure 8 we show these observables, namely the invariant mass (left) and the azimuthal-angle separation (right) of the two charged leptons, within the Higgs-background setup. As discussed above, the large relative corrections to the invariant-mass distribution of the two charged leptons in the ATLAS WW setup were observed for large $M_{e^-\mu^+}$, a region that is completely removed by the additional cuts, so that smaller EW corrections are expected. In the allowed range of the invariant mass of the charged-lepton system we now observe quite uniformly distributed corrections from all contributions (figure 8, left). For the azimuthal-angle separation (figure 8, right), the region of phase space exhibiting the most pronounced EW corrections in the ATLAS WW setup has been cut away, but the cuts affect the LO distribution and the corrections in the allowed range in a non-trivial way. Towards the new maximal value of $\Delta\phi_{e^-\mu^+}^{\mathrm{cut}} = 1.8$ we observe a strong decrease of the cross section and a reduction of the EW corrections.
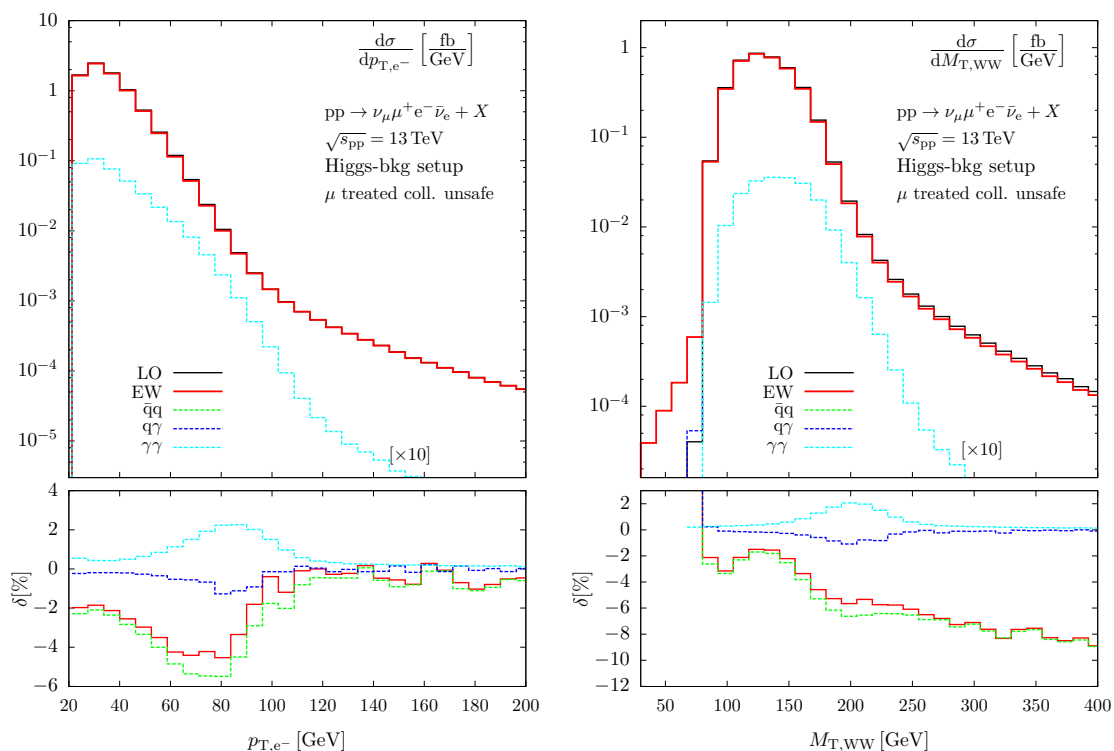
Figure 9. Transverse-momentum distribution of the electron (left) and transverse-mass distribution of the four-lepton system (right) in pp $\to \nu_\mu \mu^+ e^- \bar{\nu}_e + X$ in the Higgs-background setup. The lower panels show the relative impact of the various contributions. Note that the $\gamma\gamma$ contribution is scaled by a factor of ten only in the upper panels.

The transverse-momentum distribution of the electron and the transverse-mass distribution of the W-pair in the Higgs-background setup are shown in figure 9. We point out that both observables exhibit a much steeper decrease of the LO cross section in the shown kinematic range than within the ATLAS WW setup (cf. figures 5 and 6): the distributions in the Higgs setup drop faster with increasing scales by roughly a factor of 100 compared to the situation in the ATLAS WW setup. The corrections induced by the $q\gamma$ and $\gamma\gamma$ channels almost cancel each other at low and are suppressed at large scales. The EW corrections are thus almost entirely due to corrections to the $\bar{q}q$ channels. They distort the shapes of the distributions significantly in a non-trivial way. While the EW corrections to the $M_{\mathrm{T,WW}}$ distribution (figure 9, right) show the onset of the typical decrease towards larger scales, the EW corrections to the $p_{\mathrm{T,e^-}}$ distribution are significant only for $p_{\mathrm{T,e^-}} \lesssim 100\,\mathrm{GeV}$.

In figure 10 we investigate the (experimentally unobservable) invariant-mass distribution of the four-lepton system, where the Higgs-boson resonance is located at $M_{\mathrm{WW}} = M_{\mathrm{H}} \approx 125\,\mathrm{GeV}$. Between $M_{\mathrm{WW}} = 80\,\mathrm{GeV}$ and the on-shell W-pair threshold at $M_{\mathrm{WW}} = 2M_{\mathrm{W}} \approx 160\,\mathrm{GeV}$, we observe a very strong increase by almost five orders of magnitude in the M_{WW} distribution. Although we clearly see that the direct production of a W-boson pair within the Higgs-background setup is still dominated by on-shell W-pairs
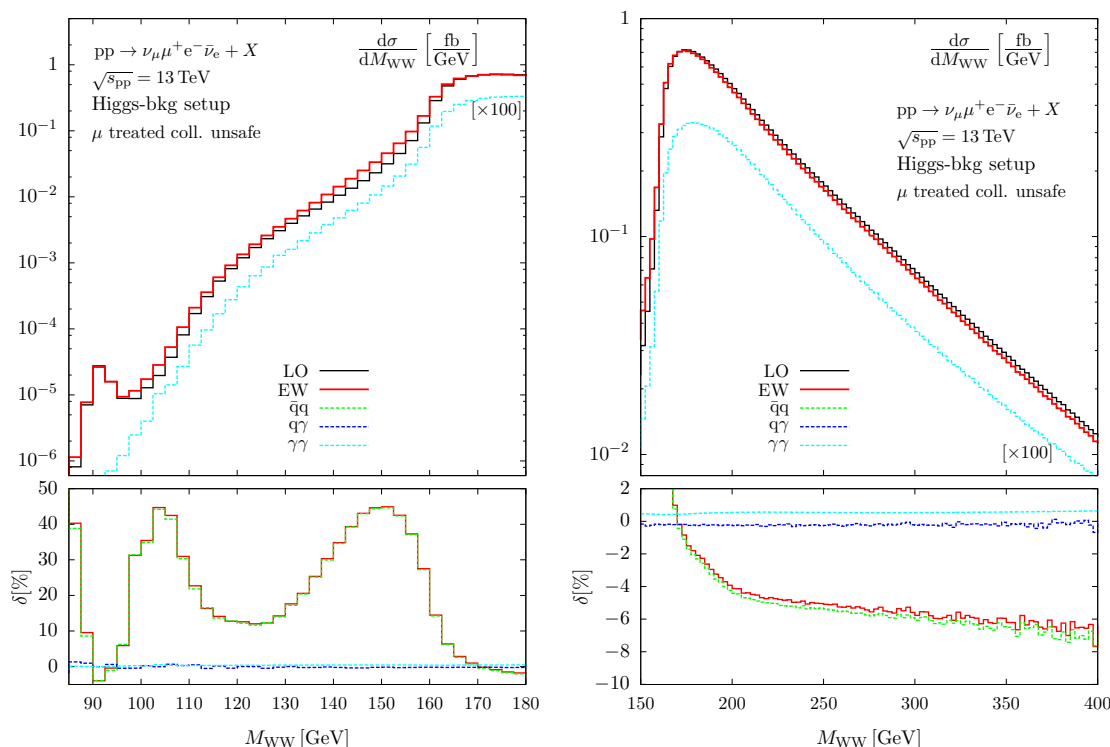
Figure 10. Invariant-mass distribution of the four-lepton system in two different plot ranges in pp → $\nu_\mu \mu^+ e^- \bar{\nu}_e$ + X in the Higgs-background setup. The lower panels show the relative impact of the various contributions. Note that the $\gamma\gamma$ contribution is scaled by a factor of hundred only in the upper panels.

with $M_{WW} \gtrsim 2M_W$, it is still interesting to look into the region below this threshold, where at least one of the W bosons is forced to be off shell. At $M_{WW} = M_Z$, the Z-boson resonance is visible, though very strongly suppressed, since at least one of the W bosons has to be far off shell there. The distinct structures and the strong positive enhancement of the EW corrections below the W-pair threshold can be attributed to the kinematic redistribution of events by collinear final-state radiation of photons off the charged leptons. This effect systematically shifts events to lower values of M_{WW}, leading to pronounced positive corrections where the spectrum falls off steeply with decreasing values of M_{WW}. This well-known feature near kinematical thresholds has recently also been discussed in a similar setup for the EW corrections for off-shell Z-pair production [47]. At the invariant W-pair mass of the order of the Higgs-boson mass of 125 GeV we observe a positive EW correction of about +15%, but we remind the reader that M_{WW} is not an observable for purely leptonically decaying W-boson pairs, in contrast to the respective situation for Z-boson pairs. Above the WW threshold, where resonant W bosons dominate, the EW correction shows again the tendency to grow into the negative direction with increasing M_{WW}. We point out, however, that this growth is much slower than observed in the transverse-momentum and transverse-mass distributions (in particular in the ATLAS WW

LHC 13 TeV	$\sigma_{\bar{q}q}^{\mathrm{LO}}$ [fb]	$\delta_{\bar{q}q}^{\mathrm{coll.\ unsafe}}$ [%]	$\delta_{\bar{q}q}^{\mathrm{coll.\ safe}}$ [%]
inclusive	390.59(3)	-3.41	-2.91
ATLAS WW	271.63(1)	-3.71	-3.18
Higgs bkg	49.934(2)	-2.54	-1.95

Table 2. LO cross sections for pp $\rightarrow \nu_\mu \mu^+ \mathrm{e}^- \bar{\nu}_\mathrm{e} + X$ at the LHC running at 13 TeV in the inclusive cut scenario (top line), the ATLAS WW setup (middle line), and the Higgs-background setup (bottom line). In the last two columns we list the relative corrections to the $\bar{q}q$-induced contributions in our default setup (collinear unsafe) and the collinear-safe setup. The numbers in brackets represent the numerical error on the last given digit.

setup, cf. figures 5 and 6), because the region of large invariant mass M_{WW} is dominated by forward-scattered W bosons owing to t-channel diagrams, and thus not by the Sudakov regime where all momentum invariants have to be large. Finally, we note that corrections due to the photon-induced channels do not play a significant role in this distribution.

3.6 Collinear-safe versus collinear-unsafe case

In this section we discuss the impact of the recombination of nearly collinear photons with final-state leptons on total and differential cross sections. In all results shown up to now, the recombination procedure described at the end of section 3.1 was applied only to electrons, while muons were treated in a collinear-unsafe way. In table 2 we list $\sigma_{\bar{q}q}^{\mathrm{LO}}$ for our three phenomenological cut scenarios at the LHC operating at an energy of $\sqrt{s_{\mathrm{pp}}} = 13$ TeV, together with the corrections from the $\bar{q}q$-induced channels for our default setup (collinear-unsafe case) and for the case where we apply the recombination procedure to both charged leptons (collinear-safe case). For integrated cross sections we observe slightly reduced corrections (by about 0.5%) in all three cut scenarios in the fully collinear-safe setup. This is due to the missing enhancement of final-state radiation by the mass singularity that appears in the collinear-unsafe treatment of muons. In the fully collinear-safe case more muons pass the cuts (after recombination with photons), so that the correction tends to be less negative.

This effect can most directly be observed in the transverse-momentum distribution of the muon and in the W-pair invariant-mass distribution, which are both shown in figure 11 in the ATLAS WW setup. In the p_{T,μ^+} distribution, which is widely monotonically falling, the collinear-unsafe correction factor signals larger negative corrections than its collinear-safe counterpart over the entire plot range, apart from the first bins where the maximum of the distribution is located. In the M_{WW} distribution the converse situation is observed: for $M_{\mathrm{WW}} \gtrsim 165-175$ GeV, where the distribution is rather flat, hardly any difference between collinear-unsafe and collinear-safe event selection is visible, because events are shifted more or less uniformly by photon recombination. For $M_{\mathrm{WW}} \lesssim 2M_{\mathrm{W}}$, however, much more events migrate from larger to smaller invariant masses in the collinear-unsafe case because of the mass-singular enhancement of final-state radiation, leading to larger positive corrections as compared to the collinear-safe case.
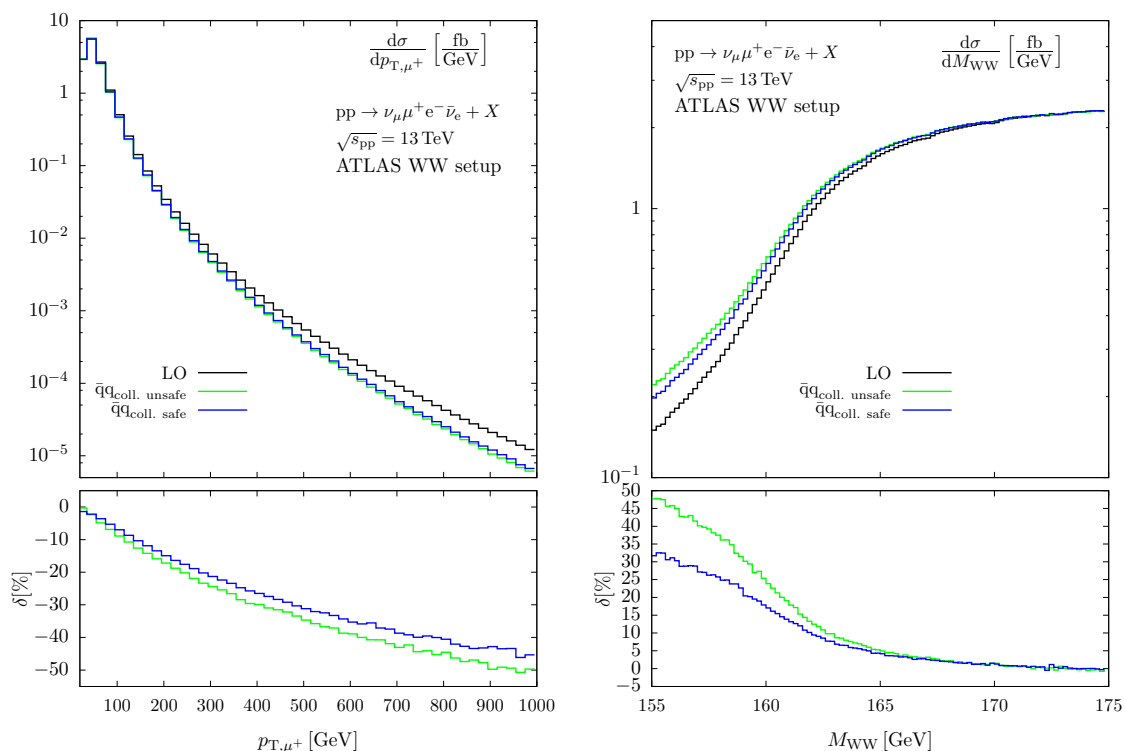
Figure 11. Transverse-momentum distribution of the muon (left) and invariant-mass distribution of the four-lepton system (right) in pp → $\nu_\mu \mu^+ e^- \bar\nu_e + X$ in the ATLAS WW setup. The lower panels show the relative size of the $\bar{q}q$ contribution within our default (collinear-unsafe) setup compared to the collinear-safe case.

Angular distributions in the final-state leptons (not shown) do not exhibit significant distortions when applying the recombination procedure, since recombining leptons and collinear photons does not systematically change the lepton direction. The difference between the two treatments directly reflects the difference observed in the integrated results over the full phase space.

3.7 Comparison to the double-pole approximation

In this section we discuss the validity and quality of the DPA, which was constructed for the virtual EW corrections to hadronic W-pair production in ref. [37], by comparing integrated and differential results in DPA to results of our full $4f$ calculation. In table 3 we list the LO cross sections $\sigma_{\bar{q}q}^{\mathrm{LO}}$ and $\sigma_{\bar{q}q}^{\mathrm{LO,DPA}}$, for our three setups at the LHC at an energy of $\sqrt{s_{\mathrm{pp}}} = 13\,\mathrm{TeV}$. The cross section $\sigma_{\bar{q}q}^{\mathrm{LO,DPA}}$ includes only doubly-resonant diagrams for the $\bar{q}q$-induced contributions. The difference of approximately 2% indicates that non-doubly-resonant contributions only contribute at the expected level of $\mathcal{O}(\Gamma_{\mathrm{W}}/M_{\mathrm{W}})$, which is, however, not good enough to achieve percent-level accuracy even after including higher-order corrections. Note that we include the DPA LO cross section $\sigma_{\bar{q}q}^{\mathrm{LO,DPA}}$ in our discussion for illustration only, but that the full $4f$ LO cross section $\sigma_{\bar{q}q}^{\mathrm{LO}}$ was consistently used in the

LHC 13 TeV	$\sigma_{\bar{q}q}^{\mathrm{LO}}$ [fb]	$\sigma_{\bar{q}q}^{\mathrm{LO,DPA}}$ [fb]	$\delta_{\bar{q}q}$ [%]	$\delta_{\bar{q}q}^{\mathrm{DPA}}$ [%]
inclusive	390.59(3)	384.96(9)	-3.41	-3.43
ATLAS WW	271.63(1)	265.31(3)	-3.71	-3.68
Higgs bkg	49.934(2)	48.88(2)	-2.54	-2.54

Table 3. LO cross sections for pp $\to \nu_\mu \mu^+ \mathrm{e}^- \bar{\nu}_\mathrm{e} + X$ at the LHC running at 13 TeV in the inclusive setup (top line), the ATLAS WW setup (middle line), and the Higgs-background setup (bottom line). In the last two columns we list the relative EW corrections to the $\bar{q}q$-induced contributions including the full virtual corrections ($\delta_{\bar{q}q}$) and applying the DPA within the virtual contributions ($\delta_{\bar{q}q}^{\mathrm{DPA}}$), both normalized to $\sigma_{\bar{q}q}^{\mathrm{LO}}$. The numbers in brackets represent the numerical error on the last given digit.

evaluation of the DPA NLO cross section in ref. [37]. As discussed already in section 2.2, we define the relative corrections of the full $4f$ prediction and the DPA upon normalizing to the full LO cross section,

$$\delta_{\bar{q}q}(\mathcal{O}) = \frac{\mathrm{d}\sigma_{\bar{q}q}^{\mathrm{NLO}}}{\mathrm{d}\mathcal{O}} \Big/ \frac{\mathrm{d}\sigma_{\bar{q}q}^{\mathrm{LO}}}{\mathrm{d}\mathcal{O}}, \qquad \delta_{\bar{q}q}^{\mathrm{DPA}}(\mathcal{O}) = \frac{\mathrm{d}\sigma_{\bar{q}q}^{\mathrm{NLO,DPA}}}{\mathrm{d}\mathcal{O}} \Big/ \frac{\mathrm{d}\sigma_{\bar{q}q}^{\mathrm{LO}}}{\mathrm{d}\mathcal{O}}, \tag{3.24}$$

so that they only differ within the virtual contributions of the NLO calculation. For integrated cross sections, the two corrections show very good agreement, as can be seen in the rightmost columns of table 3.

A similar observation can be made for the rapidity distributions of the leptons, which is illustrated for the one of the electron on the l.h.s. of figure 12 in the ATLAS WW setup. In the upper panel we observe the clear deviation of $\sigma_{\bar{q}q}^{\mathrm{LO,DPA}}$ from the full LO prediction, being of the same order of magnitude as the EW corrections to the $\bar{q}q$-induced processes. The lower panel shows the excellent agreement of the two versions for the relative corrections, with differences at the 0.1% level only.

The r.h.s. of figure 12 illustrates the same comparison for the invariant-mass distribution of the charged-lepton system in the ATLAS WW setup. For $M_{\mathrm{e}^-\mu^+} \lesssim 500\,\mathrm{GeV}$, the DPA is accurate within 1%, but the difference grows to about 2−3% in the TeV range. This increasing difference between the full $4f$ calculation and the DPA can already be inferred from the LO cross sections $\sigma_{\bar{q}q}^{\mathrm{LO}}$ and $\sigma_{\bar{q}q}^{\mathrm{LO,DPA}}$ in the upper panel, which signals the increasing impact of singly-resonant contributions not being included in the DPA. The difference between full and DPA NLO EW corrections is well covered by the last term of our estimate eq. (2.6). In view of the typically expected accuracies in LHC data analyses, the DPA is certainly sufficient for this observable.
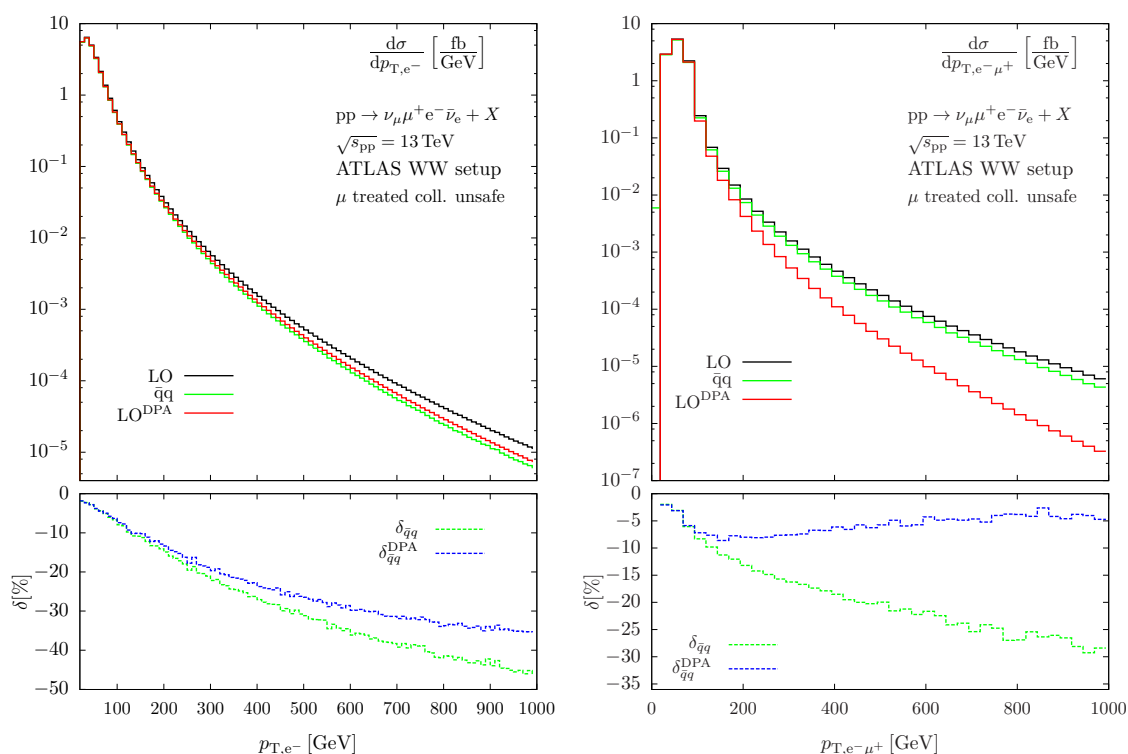
Finally, in figure 13 we turn to the transverse-momentum distributions of the electron (left) and the charged-lepton system (right). In the $p_{\mathrm{T,e}^-}$ distribution, the comparison between full and DPA calculation reveals similar qualitative features as for the $M_{\mathrm{e}^-\mu^+}$ distribution. The differences are, however, larger in size, reaching the 5% (10%) level for transverse momenta $p_{\mathrm{T,e}^-}$ of about 500 GeV (1 TeV). Again the deterioration of the DPA can already be seen at LO and attributed to an enhanced impact of the singly-resonant background diagrams shown in the second line of figure 1, which are not included

– 23 –
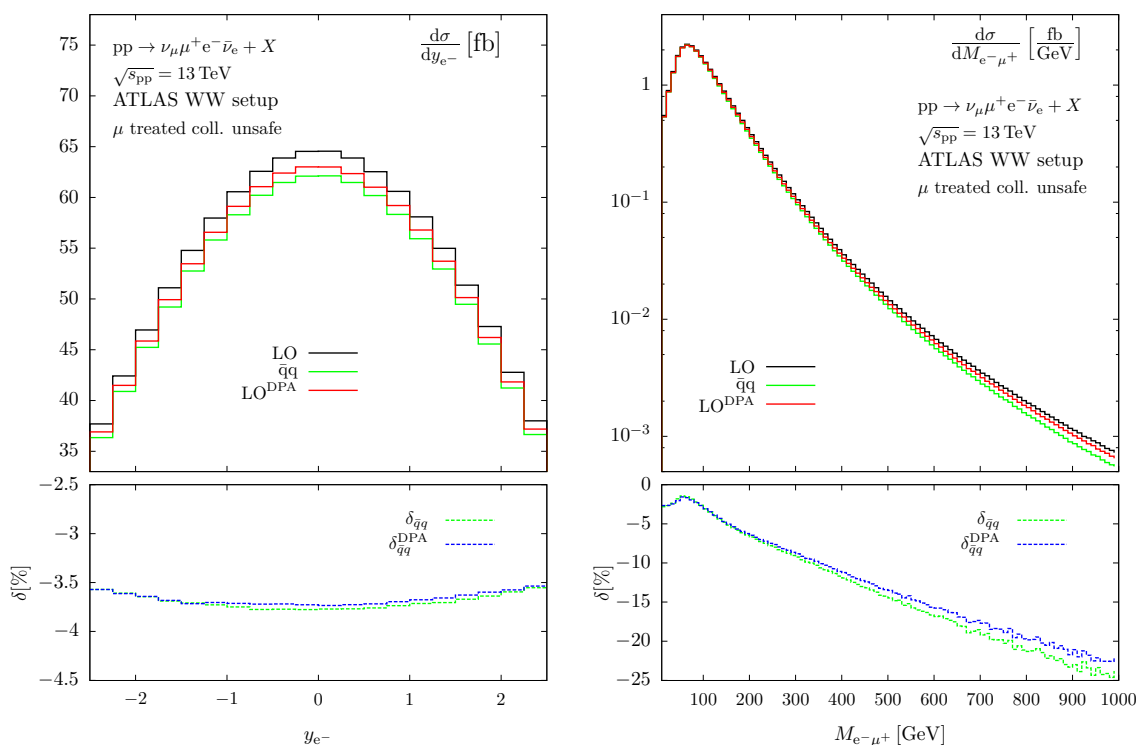
Figure 12. Rapidity distribution of the electron (left) and invariant-mass distribution of the charged-lepton system (right) in pp → $\nu_\mu\mu^+e^-\bar{\nu}_e + X$ in the ATLAS WW setup. The lower panels show the relative size of the EW corrections to the $\bar{q}q$ channels in our default setup compared to the result based on the DPA.

in $\sigma_{\bar{q}q}^{\mathrm{LO,DPA}}$. Schematically the relevant diagrams are kinematically illustrated on the l.h.s. of figure 14. The enhancement is due to events where one single lepton is recoiling against the other three in the final state. Thus, for large $p_{\mathrm{T,e^-}}$ the cross section $\mathrm{d}\sigma_{\bar{q}q}^{\mathrm{LO}}/\mathrm{d}p_{\mathrm{T,e^-}}$ receives large contributions from events where the electron is back-to-back to the three other leptons. For doubly-resonant diagrams (first line in figure 1) this situation is less likely for large $p_{\mathrm{T,e^-}}$, where the W-decay lepton pairs mostly appear back-to-back as a result of the boost from the W rest frames to the laboratory system. The comparison of $\sigma_{\bar{q}q}^{\mathrm{LO}}$ with $\sigma_{\bar{q}q}^{\mathrm{LO,DPA}}$ at high $p_{\mathrm{T,e^-}}$ shows that singly-resonant contributions dominate over doubly-resonant parts already for a $p_{\mathrm{T,e^-}}$ of some 100 GeV. Kinematically, it is thus easier to produce leptons with high transverse momenta directly rather than through the decay of W bosons. The difference between full and DPA NLO EW corrections is again reproduced quite well by the last term of our estimate eq. (2.6).

The difference between the full $4f$ and the DPA calculation is pushed to the extreme in the distribution of the transverse momentum $p_{\mathrm{T,e^-\mu^+}}$ of the charged-lepton system. Here the enhancement of background diagrams is due to events where one neutrino recoils against the two charged leptons and the other neutrino, a situation that is supported by singly-resonant diagrams as illustrated on the r.h.s. of figure 14, but not by doubly-resonant

Figure 13. Transverse-momentum distributions of the electron (left) and of the charged-lepton system (right) in pp $\to \nu_\mu \mu^+ e^- \bar{\nu}_e + X$ in the ATLAS WW setup. The lower panels show the relative size of the EW corrections to the $\bar{q}q$ channels in our default setup compared to the result based on the DPA.
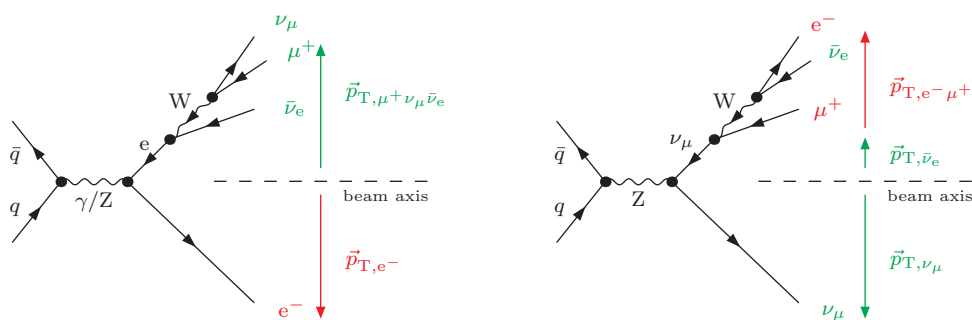
Figure 14. Illustration of diagrammatic structures dominating the p_{T,e^-} (left) and $p_{T,e^-\mu^+}$ (right) distributions shown in figure 13 for high transverse momenta.

graphs, where the two charged leptons tend to recoil against each other for high transverse momenta. Looking at equal sizes of transverse momenta on the horizontal axes of the two distributions in figure 13, the enhancement seems stronger in the case of the $p_{T,e^-\mu^+}$ distribution, but at the same time it should be realized that the spectrum on the r.h.s. drops much faster than the one of p_{T,e^-} on the l.h.s. for increasing p_T. This is due to the fact that $p_{T,e^-\mu^+}$ contains only part of the transverse momentum of the three-lepton

system recoiling against the single neutrino and that it is very unlikely to produce a large $p_{\mathrm{T,e^-\mu^+}}$ via the doubly resonant contributions. In conclusion, we can state that transverse-momentum distributions are reproduced by the DPA only up to some $100\,\mathrm{GeV}$ owing to the growing influence of background diagrams that do not show two simultaneously resonant W bosons. For predictions of such p_{T} spectra in the TeV range, the calculation of EW corrections should be based on a full 4-fermion calculation.

4 Conclusions and outlook

Electroweak di-boson production processes represent a very interesting class of particle reactions at the LHC. They provide an ideal test-ground for the non-Abelian self-interactions among the electroweak gauge bosons, but also form an important class of backgrounds to many new-physics searches and to precision studies of the Higgs boson. Precise calculations for these processes, including radiative corrections of strong and electroweak interactions, are thus phenomenologically very important and have seen great progress in recent years. On the one hand, QCD predictions are being pushed to the next-to-next-to-leading-order level and are extended by including leading corrections beyond fixed orders. On the other hand, calculations of electroweak corrections become more and more refined by including decays of the unstable bosons and off-shell effects.

In this paper, we have reported the results from the first calculation of next-to-leading-order electroweak corrections to W-boson pair production that fully takes into account leptonic W-boson decays and off-shell effects. This calculation is based on the complex-mass scheme for the treatment of the intermediate electroweak gauge bosons and provides next-to-leading-order precision over the entire phase space with resonant and/or non-resonant W bosons. Thus, it goes beyond previous calculations which are restricted to on-shell or nearly resonant W bosons.

We have discussed the electroweak corrections using different event selections, comprising one that is typical for the study of W-boson pairs as a signal process and another one that is typical for an analysis of Higgs-boson decays $\mathrm{H} \to \mathrm{WW}^*$, where W-boson pair production represents an irreducible background. In particular, we have compared the full off-shell results to previous results in the so-called double-pole approximation, which is based on an expansion of the loop amplitudes about the poles of the W resonances. At small and intermediate scales, i.e. in particular in angular and rapidity distributions, the two approaches show the expected agreement at the level of fractions of a percent, but larger differences appear for invariant-mass and transverse-momentum distributions in the TeV range. For transverse-momentum distributions, the differences can even exceed the 10% level in the TeV range where "background diagrams" with one instead of two resonant W bosons grow in importance because of the suppression of the doubly resonant contributions in these kinematical regimes.

To fully exploit our calculation in upcoming LHC data analyses, our state-of-the-art results on electroweak corrections should be combined with QCD-corrected cross sections. A simple way to achieve this, would be to apply differential reweighting factors for the electroweak corrections to differential distributions obtained with state-of-the-art QCD-

based predictions. Predictions obtained in this way would be accurate to the level of very few percent for integrated cross sections and distributions that are dominated by energy scales up to few 100 GeV. For transverse-momentum and invariant-mass distributions in the TeV range, the precision will deteriorate and most likely be limited by our knowledge of QCD corrections, while electroweak corrections are sufficiently well under control.

Acknowledgments

References

[1] ATLAS collaboration, *Measurement of W^+W^- production in pp collisions at $\sqrt{s} = 7$ TeV with the ATLAS detector and limits on anomalous WWZ and WWγ couplings*, *Phys. Rev.* **D 87** (2013) 112001 [`arXiv:1210.2979`] [iNSPIRE].

[2] ATLAS collaboration, *Measurement of the WW + WZ cross section and limits on anomalous triple gauge couplings using final states with one lepton, missing transverse momentum and two jets with the ATLAS detector at $\sqrt{s} = 7$ TeV*, *JHEP* **01** (2015) 049 [`arXiv:1410.7238`] [iNSPIRE].

[3] CMS collaboration, *Measurement of the W^+W^- cross section in pp collisions at $\sqrt{s} = 7$ TeV and limits on anomalous WWγ and WWZ couplings*, *Eur. Phys. J.* **C 73** (2013) 2610 [`arXiv:1306.1126`] [iNSPIRE].

[4] CMS collaboration, *Measurement of the W^+W^- cross section in pp collisions at $\sqrt{s} = 8$ TeV and limits on anomalous gauge couplings*, [`arXiv:1507.03268`] [iNSPIRE].

[5] J. Ohnemus, *An order α_s calculation of hadronic W^-W^+ production*, *Phys. Rev.* **D 44** (1991) 1403 [iNSPIRE].

[6] S. Frixione, *A next-to-leading order calculation of the cross-section for the production of W^+W^- pairs in hadronic collisions*, *Nucl. Phys.* **B 410** (1993) 280 [iNSPIRE].

[7] U. Baur, T. Han and J. Ohnemus, *QCD corrections and nonstandard three vector boson couplings in W^+W^- production at hadron colliders*, *Phys. Rev.* **D 53** (1996) 1098 [`hep-ph/9507336`] [iNSPIRE].

[8] L.J. Dixon, Z. Kunszt and A. Signer, *Helicity amplitudes for $O(\alpha_s)$ production of W^+W^-, $W^\pm Z$, ZZ, $W^\pm\gamma$, or $Z\gamma$ pairs at hadron colliders*, *Nucl. Phys.* **B 531** (1998) 3 [hep-ph/9803250] [INSPIRE].

[9] J.M. Campbell and R.K. Ellis, *An update on vector boson pair production at hadron colliders*, *Phys. Rev.* **D 60** (1999) 113006 [hep-ph/9905386] [INSPIRE].

[10] S. Frixione and B.R. Webber, *Matching NLO QCD computations and parton shower simulations*, *JHEP* **06** (2002) 029 [hep-ph/0204244] [INSPIRE].

[11] K. Hamilton, *A positive-weight next-to-leading order simulation of weak boson pair production*, *JHEP* **01** (2011) 009 [arXiv:1009.5391] [INSPIRE].

[12] S. Höche, F. Krauss, M. Schönherr and F. Siegert, *Automating the POWHEG method in Sherpa*, *JHEP* **04** (2011) 024 [arXiv:1008.5399] [INSPIRE].

[13] T. Melia, P. Nason, R. Röntsch and G. Zanderighi, *W^+W^-, WZ and ZZ production in the POWHEG BOX*, *JHEP* **11** (2011) 078 [arXiv:1107.5051] [INSPIRE].

[14] R. Frederix, S. Frixione, V. Hirschi, F. Maltoni, R. Pittau and P. Torrielli, *Four-lepton production at hadron colliders: aMC@NLO predictions with theoretical uncertainties*, *JHEP* **02** (2012) 099 [arXiv:1110.4738] [INSPIRE].

[15] P. Nason and G. Zanderighi, *W^+W^-, WZ and ZZ production in the POWHEG-BOX-V2*, *Eur. Phys. J.* **C 74** (2014) 2702 [arXiv:1311.1365] [INSPIRE].

[16] T. Gehrmann et al., *W^+W^- production at hadron colliders in next to next to leading order QCD*, *Phys. Rev. Lett.* **113** (2014) 212001 [arXiv:1408.5243] [INSPIRE].

[17] M. Grazzini, S. Kallweit, S. Pozzorini, D. Rathlev and M. Wiesemann, *W^+W^- production at the LHC: fiducial cross sections and distributions in NNLO QCD*, arXiv:1605.02716 [INSPIRE].

[18] G. Chachamis, M. Czakon and D. Eiras, *W pair production at the LHC. I. Two-loop corrections in the high energy limit*, *JHEP* **12** (2008) 003 [arXiv:0802.4028] [INSPIRE].

[19] G. Chachamis, M. Czakon and D. Eiras, *W pair production at the LHC. II. One-loop squared corrections in the high energy limit*, arXiv:0806.3043 [INSPIRE].

[20] M. Grazzini, *Soft-gluon effects in WW production at hadron colliders*, *JHEP* **01** (2006) 095 [hep-ph/0510337] [INSPIRE].

[21] S. Dawson, I.M. Lewis and M. Zeng, *Threshold resummed and approximate next-to-next-to-leading order results for W^+W^- pair production at the LHC*, *Phys. Rev.* **D 88** (2013) 054028 [arXiv:1307.3249] [INSPIRE].

[22] Y. Wang, C.S. Li, Z.L. Liu, D.Y. Shao and H.T. Li, *Transverse-momentum resummation for gauge boson pair production at the hadron collider*, *Phys. Rev.* **D 88** (2013) 114017 [arXiv:1307.7520] [INSPIRE].

[23] D.A. Dicus, C. Kao and W.W. Repko, *Gluon production of gauge bosons*, *Phys. Rev.* **D 36** (1987) 1570 [INSPIRE].

[24] E.W.N. Glover and J.J. van der Bij, *Vector boson pair production via gluon fusion*, *Phys. Lett.* **B 219** (1989) 488 [INSPIRE].

[25] T. Binoth, M. Ciccolini, N. Kauer and M. Krämer, *Gluon-induced WW background to Higgs boson searches at the LHC*, *JHEP* **03** (2005) 065 [hep-ph/0503094] [INSPIRE].

[26] T. Binoth, M. Ciccolini, N. Kauer and M. Krämer, *Gluon-induced W-boson pair production at the LHC*, *JHEP* **12** (2006) 046 [hep-ph/0611170] [INSPIRE].

[27] T. Melia, K. Melnikov, R. Röntsch, M. Schulze and G. Zanderighi, *Gluon fusion contribution to W^+W^- + jet production*, *JHEP* **08** (2012) 115 [arXiv:1205.6987] [INSPIRE].

[28] J. Bellm et al., *Anomalous coupling, top-mass and parton-shower effects in W^+W^- production*, arXiv:1602.05141 [INSPIRE].

[29] F. Cascioli, S. Höche, F. Krauss, P. Maierhöfer, S. Pozzorini and F. Siegert, *Precise Higgs-background predictions: merging NLO QCD and squared quark-loop corrections to four-lepton + 0,1 jet production*, *JHEP* **01** (2014) 046 [arXiv:1309.0500] [INSPIRE].

[30] F. Caola, K. Melnikov, R. Röntsch and L. Tancredi, *QCD corrections to W^+W^- production through gluon fusion*, *Phys. Lett.* **B 754** (2016) 275 [arXiv:1511.08617] [INSPIRE].

[31] E. Accomando, A. Denner and A. Kaiser, *Logarithmic electroweak corrections to gauge-boson pair production at the LHC*, *Nucl. Phys.* **B 706** (2005) 325 [hep-ph/0409247] [INSPIRE].

[32] E. Accomando and A. Kaiser, *Electroweak corrections and anomalous triple gauge-boson couplings in W^+W^- and $W^\pm Z$ production at the LHC*, *Phys. Rev.* **D 73** (2006) 093006 [hep-ph/0511088] [INSPIRE].

[33] J.H. Kühn, F. Metzler, A.A. Penin and S. Uccirati, *Next-to-next-to-leading electroweak logarithms for W-pair production at LHC*, *JHEP* **06** (2011) 143 [arXiv:1101.2563] [INSPIRE].

[34] A. Bierweiler, T. Kasprzik, J.H. Kühn and S. Uccirati, *Electroweak corrections to W-boson pair production at the LHC*, *JHEP* **11** (2012) 093 [arXiv:1208.3147] [INSPIRE].

[35] A. Bierweiler, T. Kasprzik and J.H. Kühn, *Vector-boson pair production at the LHC to $\mathcal{O}(\alpha^3)$ accuracy*, *JHEP* **12** (2013) 071 [arXiv:1305.5402] [INSPIRE].

[36] J. Baglio, L.D. Ninh and M.M. Weber, *Massive gauge boson pair production at the LHC: a next-to-leading order story*, *Phys. Rev.* **D 88** (2013) 113005 [arXiv:1307.4331] [INSPIRE].

[37] M. Billóni, S. Dittmaier, B. Jäger and C. Speckner, *Next-to-leading order electroweak corrections to $pp \to W^+W^- \to 4$ leptons at the LHC in double-pole approximation*, *JHEP* **12** (2013) 043 [arXiv:1310.1564] [INSPIRE].

[38] S. Gieseke, T. Kasprzik and J.H. Kühn, *Vector-boson pair production and electroweak corrections in HERWIG++*, *Eur. Phys. J.* **C 74** (2014) 2988 [arXiv:1401.3964] [INSPIRE].

[39] M. Dyndal and L. Schoeffel, *Four-lepton production from photon-induced reactions in pp collisions at the LHC*, arXiv:1511.02065 [INSPIRE].

[40] M. Luszczak and A. Szczurek, *Subleading processes in production of W^+W^- pairs in proton-proton collisions*, arXiv:1309.7201 [INSPIRE].

[41] NNPDF collaboration, R.D. Ball et al., *Parton distributions with QED corrections*, *Nucl. Phys.* **B 877** (2013) 290 [arXiv:1308.0598] [INSPIRE].

[42] A. Denner, S. Dittmaier, M. Roth and L.H. Wieders, *Complete electroweak $O(\alpha)$ corrections to charged-current $e^+e^- \to 4$ fermion processes*, *Phys. Lett.* **B 612** (2005) 223 [*Erratum ibid.* **B 704** (2011) 667] [hep-ph/0502063] [INSPIRE].

[43] A. Denner, S. Dittmaier, M. Roth and L.H. Wieders, *Electroweak corrections to charged-current $e^+e^- \to 4$ fermion processes: technical details and further results*, *Nucl. Phys.* **B 724** (2005) 247 [*Erratum ibid.* **B 854** (2012) 504] [hep-ph/0505042] [INSPIRE].

[44] A. Denner, S. Dittmaier, M. Roth and D. Wackeroth, *$O(\alpha)$ corrections to $e^+e^- \to WW \to$ four fermions $(+\gamma)$: first numerical results from RACOON WW*, *Phys. Lett.* **B 475** (2000) 127 [hep-ph/9912261] [INSPIRE].

[45] A. Denner, S. Dittmaier, M. Roth and D. Wackeroth, *Electroweak radiative corrections to* $e^+e^- \to WW \to 4$ *fermions in double pole approximation: The RACOONWW approach*, *Nucl. Phys.* **B 587** (2000) 67 [hep-ph/0006307] [INSPIRE].

[46] A. Denner, S. Dittmaier, M. Roth and D. Wackeroth, *RACOONWW1.3: A Monte Carlo program for four fermion production at* e^+e^- *colliders*, *Comput. Phys. Commun.* **153** (2003) 462 [hep-ph/0209330] [INSPIRE].

[47] B. Biedermann, A. Denner, S. Dittmaier, L. Hofer and B. Jäger, *Electroweak corrections to* $pp \to \mu^+\mu^- e^+e^- + X$ *at the LHC: a Higgs background study*, *Phys. Rev. Lett.* **116** (2016) 161803 [arXiv:1601.07787] [INSPIRE].

[48] S. Actis, A. Denner, L. Hofer, A. Scharf and S. Uccirati, *Recursive generation of one-loop amplitudes in the Standard Model*, *JHEP* **04** (2013) 037 [arXiv:1211.6316] [INSPIRE].

[49] S. Actis, A. Denner, L. Hofer, J.-N. Lang, A. Scharf and S. Uccirati, *RECOLA: REcursive Computation of One-Loop Amplitudes*, arXiv:1605.01090 [INSPIRE].

[50] A. Denner, S. Dittmaier and L. Hofer, *COLLIER — A fortran-library for one-loop integrals*, PoS(LL2014)071 [arXiv:1407.0087] [INSPIRE].

[51] A. Denner, S. Dittmaier and L. Hofer, *Collier: a fortran-based Complex one-loop LIbrary in Extended Regularizations*, arXiv:1604.06792 [INSPIRE].

[52] A. Denner, S. Dittmaier, M. Roth and D. Wackeroth, *Predictions for all processes* $e^+e^- \to 4$ *fermions* $+ \gamma$, *Nucl. Phys.* **B 560** (1999) 33 [hep-ph/9904472] [INSPIRE].

[53] A. Denner and S. Dittmaier, *The complex-mass scheme for perturbative calculations with unstable particles*, *Nucl. Phys. Proc. Suppl.* **160** (2006) 22 [hep-ph/0605312] [INSPIRE].

[54] A. Bredenstein, S. Dittmaier and M. Roth, *Four-fermion production at gamma gamma colliders. 2. Radiative corrections in double-pole approximation*, *Eur. Phys. J.* **C 44** (2005) 27 [hep-ph/0506005] [INSPIRE].

[55] J. Küblbeck, M. Böhm and A. Denner, *Feyn Arts: computer algebraic generation of Feynman graphs and amplitudes*, *Comput. Phys. Commun.* **60** (1990) 165 [INSPIRE].

[56] T. Hahn, *Generating Feynman diagrams and amplitudes with FeynArts 3*, *Comput. Phys. Commun.* **140** (2001) 418 [hep-ph/0012260] [INSPIRE].

[57] E. Accomando, A. Denner and C. Meier, *Electroweak corrections to* $W\gamma$ *and* $Z\gamma$ *production at the LHC*, *Eur. Phys. J.* **C 47** (2006) 125 [hep-ph/0509234] [INSPIRE].

[58] T. Hahn and M. Pérez-Victoria, *Automatized one loop calculations in four-dimensions and D-dimensions*, *Comput. Phys. Commun.* **118** (1999) 153 [hep-ph/9807565] [INSPIRE].

[59] T. Hahn, *Automatic loop calculations with FeynArts, FormCalc and LoopTools*, *Nucl. Phys. Proc. Suppl.* **89** (2000) 231 [hep-ph/0005029] [INSPIRE].

[60] A. Denner and S. Dittmaier, *Reduction of one loop tensor five point integrals*, *Nucl. Phys.* **B 658** (2003) 175 [hep-ph/0212259] [INSPIRE].

[61] A. Denner and S. Dittmaier, *Reduction schemes for one-loop tensor integrals*, *Nucl. Phys.* **B 734** (2006) 62 [hep-ph/0509141] [INSPIRE].

[62] A. Denner and S. Dittmaier, *Scalar one-loop 4-point integrals*, *Nucl. Phys.* **B 844** (2011) 199 [arXiv:1005.2076] [INSPIRE].

[63] S. Dittmaier, *A general approach to photon radiation off fermions*, *Nucl. Phys.* **B 565** (2000) 69 [hep-ph/9904440] [INSPIRE].

[64] S. Dittmaier, A. Kabelschacht and T. Kasprzik, *Polarized QED splittings of massive fermions and dipole subtraction for non-collinear-safe observables*, *Nucl. Phys.* **B 800** (2008) 146 [arXiv:0802.1405] [inSPIRE].

[65] W. Beenakker, F.A. Berends and A.P. Chapovsky, *Radiative corrections to pair production of unstable particles: results for $e^+e^- \to$ four fermions*, *Nucl. Phys.* **B 548** (1999) 3 [hep-ph/9811481] [inSPIRE].

[66] S. Jadach, W. Płaczek, M. Skrzypek, B.F.L. Ward and Z. Wąs, *Final state radiative effects for the exact $O(\alpha)$ YFS exponentiated (un)stable W^+W^- production at and beyond LEP-2 energies*, *Phys. Rev.* **D 61** (2000) 113010 [hep-ph/9907436] [inSPIRE].

[67] S. Jadach, W. Płaczek, M. Skrzypek, B.F.L. Ward and Z. Wąs, *The Monte Carlo event generator YFSWW3 version 1.16 for W pair production and decay at LEP-2/LC energies*, *Comput. Phys. Commun.* **140** (2001) 432 [hep-ph/0103163] [inSPIRE].

[68] M.W. Grünewald et al., *Reports of the Working Groups on Precision Calculations for LEP2 Physics: Proceedings. Four fermion production in electron positron collisions*, hep-ph/0005309 [inSPIRE].

[69] S. Dittmaier and C. Schwan, *Non-factorizable photonic corrections to resonant production and decay of many unstable particles*, *Eur. Phys. J.* **C 76** (2016) 144 [arXiv:1511.01698] [inSPIRE].

[70] PARTICLE DATA GROUP collaboration, J. Beringer et al., *Review of Particle Physics (RPP)*, *Phys. Rev.* **D 86** (2012) 010001 [inSPIRE].

[71] D. Yu. Bardin, A. Leike, T. Riemann and M. Sachwitz, *Energy-dependent width effects in e^+e^- annihilation near the Z boson pole*, *Phys. Lett.* **B 206** (1988) 539 [inSPIRE].

[72] K.P.O. Diener, S. Dittmaier and W. Hollik, *Electroweak higher-order effects and theoretical uncertainties in deep-inelastic neutrino scattering*, *Phys. Rev.* **D 72** (2005) 093002 [hep-ph/0509084] [inSPIRE].

[73] ATLAS collaboration, *Measurement of the transverse momentum distribution of Z/γ^* bosons in proton-proton collisions at $\sqrt{s} = 7$ TeV with the ATLAS detector*, *Phys. Lett.* **B 705** (2011) 415 [arXiv:1107.2381] [inSPIRE].

[74] ATLAS collaboration, *Observation and measurement of Higgs boson decays to WW^* with the ATLAS detector*, *Phys. Rev.* **D 92** (2015) 012006 [arXiv:1412.2641] [inSPIRE].

[75] CMS collaboration, *Measurement of Higgs boson production and properties in the WW decay channel with leptonic final states*, *JHEP* **01** (2014) 096 [arXiv:1312.1129] [inSPIRE].

[76] M. Rubin, G.P. Salam and S. Sapeta, *Giant QCD K-factors beyond NLO*, *JHEP* **09** (2010) 084 [arXiv:1006.2144] [inSPIRE].

[77] ATLAS collaboration, *Search for the Standard Model Higgs boson in the $H \to WW(*) \to \ell\nu\ell\nu$ decay mode with 4.7/fb of ATLAS data at $\sqrt{s} = 7$ TeV*, *Phys. Lett.* **B 716** (2012) 62 [arXiv:1206.0756] [inSPIRE].